Journal of Cell Biology

ARTICLE

NF-κB disinhibition contributes to dendrite defects in fly models of neurodegenerative diseases

Myeong Hoon Han[1]*, Min Jee Kwon[1]*, Byung Su Ko[1]*, Do Young Hyeon[2], Davin Lee[1], Hyung-Jun Kim[3], Daehee Hwang[2], and Sung Bae Lee[1,4,5]

Dendrite pathology is frequently observed in various neurodegenerative diseases (NDs). Although previous studies identified several pathogenic mediators of dendrite defects that act through loss of function in NDs, the underlying pathogenic mechanisms remain largely unexplored. Here, our search for additional pathogenic contributors to dendrite defects in NDs identifies Relish/NF-κB as a novel gain-of-toxicity–based mediator of dendrite defects in animal models for polyglutamine (polyQ) diseases and amyotrophic lateral sclerosis (ALS). In a *Drosophila* model for polyQ diseases, polyQ-induced dendrite defects require Dredd/Caspase-8–mediated endoproteolytic cleavage of Relish to generate the N-terminal fragment, Rel68, and subsequent Charon-mediated nuclear localization of Rel68. Rel68 alone induced neuronal toxicity causing dendrite and behavioral defects, and we identify two novel transcriptional targets, Tup and Pros, that mediate Rel68-induced neuronal toxicity. Finally, we show that Rel68-induced toxicity also contributes to dendrite and behavioral defects in a *Drosophila* model for ALS. Collectively, our data propose disinhibition of latent toxicity of Relish/NF-κB as a novel pathogenic mechanism underlying dendrite pathology in NDs.

Introduction

Neurodegenerative diseases (NDs) are late-onset neurological disorders characterized by gradual loss of neuronal ability to maintain morphological integrity and functionality. Representative NDs include Alzheimer's disease (AD), Parkinson's disease (PD), polyglutamine (polyQ) diseases, and amyotrophic lateral sclerosis (ALS). The progressive impairment in various neuronal functions may be caused by the loss of function and/or gain of toxicity of associated proteins in the disease condition. Regarding the loss-of-function aspect, extensive studies have identified numerous proteins (either disease-responsible proteins or mediators of pathogenesis) whose loss of function contributes to various neuropathic features in NDs. In contrast, the gain-of-toxicity aspect has been studied with a primary focus on how accumulated misfolded proteins (e.g., amyloid β in AD, α-synuclein in PD, and polyQ proteins in polyQ diseases) gain protein toxicity in neurons upon genetic mutations or environmental factors (Chung et al., 2018). However, the involvement of additional pathogenic mediators for the gain of toxicity during disease progression has not been well studied.

Because neuronal cell death common to NDs occurs mainly at the late stages of disease progression, early neuropathic features such as morphological changes have been extensively studied to explain how disease initiates and progresses before massive neuronal cell death (Kweon et al., 2017). In line with this, dendrite defects have been frequently observed in patients and in animal models for AD (Knobloch and Mansuy, 2008; Spires et al., 2005), PD (Blumenstock et al., 2017; McNeill et al., 1988), polyQ diseases (Graveland et al., 1985; Lee et al., 2011), and ALS (Gorrie et al., 2014). Previous studies have identified several molecules whose loss of function contributes to dendrite defects in animal models for NDs originating from gain of toxicity of accumulated misfolded proteins. For example, May et al. (2014) reported that the amount of soluble UNC119 regulating dendrite morphology was reduced by poly-Gly-Ala aggregates produced by the expanded *C9orf72* nucleotide repeats, which led to dendrite defects in primary hippocampal and cortical neurons of ALS rat models. In addition, misfolded polyQ proteins induce dendrite defects in fly models for polyQ diseases by perturbing the CREB-binding protein-CREB3L1/CrebA pathway (Chung et al., 2017) or Forkhead box, subgroup O (Kwon et al., 2018).

However, whether the gain of toxicity of additional mediators (hereafter called toxic mediators) contributes to dendrite

---

[1]Department of Brain and Cognitive Sciences, Daegu Gyeongbuk Institute of Science and Technology, Daegu, Republic of Korea; [2]School of Biological Science, Seoul National University, Seoul, Republic of Korea; [3]Dementia Research Group, Korea Brain Research Institute, Daegu, Republic of Korea; [4]Protein Dynamics–Based Proteotoxicity Control Laboratory, Basic Research Lab, Daegu Gyeongbuk Institute of Science and Technology, Daegu, Korea; [5]Well Aging Research Center, Division of Biotechnology, Daegu Gyeongbuk Institute of Science and Technology, Daegu, Korea.

*M.H. Han, M.J. Kwon, and B.S. Ko contributed equally to this paper; Correspondence to Sung Bae Lee: sblee@dgist.ac.kr.

© 2020 Han et al. This article is distributed under the terms of an Attribution–Noncommercial–Share Alike–No Mirror Sites license for the first six months after the publication date (see http://www.rupress.org/terms/). After six months it is available under a Creative Commons License (Attribution–Noncommercial–Share Alike 4.0 International license, as described at https://creativecommons.org/licenses/by-nc-sa/4.0/).

Rockefeller University Press
https://doi.org/10.1083/jcb.202004107
J. Cell Biol. 2020 Vol. 219 No. 12 e202004107

defects in NDs remains to be elucidated. We therefore searched for toxic mediators by categorizing candidates using the following criteria: first, their abundance and/or functions are aberrantly up-regulated in the disease condition; second, their down-regulation or reduced expression is able to ameliorate dendrite defects in NDs. Using these criteria, we identified NF-κB as a novel toxic mediator of dendrite defects in animal models for two representative NDs, Machado-Joseph disease/spinocerebellar ataxia type 3 (MJD/SCA3) and ALS. Notably, several previous studies suggested that NF-κB harbors deleterious effects within the neuronal context in a cell-autonomous manner (Pizzi et al., 2002; Sarnico et al., 2009). For proper function of neurons, the latent toxicity of NF-κB should be under tight control to avoid unwanted damage from it. However, it remains elusive in what conditions and how neurons lose their control for NF-κB toxicity and what pathophysiological features in neuronal disorders involve dysregulation of NF-κB toxicity. Here, using *Drosophila* as a model system, we present disinhibition of NF-κB induced by perturbed Dredd/Caspase-8–mediated endoproteolytic cleavage of it as a novel pathogenic mechanism of action underlying dendrite defects in animal models for NDs and identify Tup and Pros as downstream mediators of NF-κB–induced neuronal toxicity.

Results

Relish is identified as a novel toxic mediator of MJD polyQ–induced dendrite defects

Among the NDs, we focused on MJD, a neurological disorder belonging to the polyQ disease family that is caused solely by the genetic mutation of a Q-encoding CAG repeat expansion resulting in protein toxicity (Kawaguchi et al., 1994). To identify toxic mediators in MJD, we first selected candidates using the previous RNA-sequencing data collected from mouse MJD models (GSE117028, Zeng et al., 2018; GSE108069, Toonen et al., 2018) and patient-derived induced pluripotent stem cell neurons expressing toxic MJD proteins (GSE96826; Chuang et al., 2019). Based on our assumption that toxic mediators should not be down-regulated under the disease condition for their gain of toxicity, we selected 6,748 non–down-regulated genes (Fig. 1 A). Of them, 5,995 genes were identified to be *Drosophila* homologous genes, among which 99 genes were predicted to be involved in dendrite morphogenesis based on gene ontology biological process annotation. Among these 99 genes, we selected only those that can act as a transcription factor (TF), since the formation and maintenance of complex dendrite morphology require sophisticated regulation of multiple genes, which is commonly conferred by TFs (Jan and Jan, 2010). Indeed, as shown in our previous studies (Chung et al., 2017; Kwon et al., 2018), perturbed TF activities result in aberrant regulation of the many downstream genes that are important in dendrite morphology and, therefore, contribute to polyQ-induced dendrite defects. Besides, enrichment analysis of gene ontology molecular functions (GOMFs) for the selected 99 genes revealed that transcriptional activity was the most strongly associated (Fig. 1 B). Among the 15 genes with TF activity selected, only 12 were identified to have available RNAi lines. Thus, we focused on 12 genes for subsequent experimental validation.

We next experimentally validated whether reduced expression of each of the 12 selected genes could ameliorate MJD polyQ–induced dendrite defects. To this end, we individually knocked down each gene in *Drosophila* class IV dendritic arborization (C4da) neurons expressing toxic MJD polyQ proteins (MJD-78Q) and compared the consequent dendrite phenotypes to those caused by MJD-78Q alone. Previous studies showed that MJD-78Q expression in C4da neurons induces obvious dendrite defects characterized by highly reduced terminal dendrite branches (Lee et al., 2011). Among the 12 genes examined, knockdown of only 2 (*Relish*, a *Drosophila* homologue of *NF-κB*, and *Ftz transcription factor 1* [*Ftz-f1*], a *Drosophila* homologue of *LRH-1* and *SF-1*) resulted in significant restoration of MJD-78Q–induced dendrite defects (Fig. 1, C and D; and Fig. S1 A). Because knockdown of Relish showed the largest effect, we focused on characterizing its potential role as a toxic mediator of dendrite defects. Furthermore, two additional Relish RNAi transgenes with validated efficiencies (Fig. S1 B) also showed the similar restoration effects in MJD polyQ–induced dendrite defects (Fig. S1, C and D). Because this restoration effect of Relish RNAi is not due to alteration in the amount of MJD-78Q proteins (Fig. S1, E–H), it can be suggested that the restoration effect of Relish RNAi may due to reduced amount of Relish in toxic MJD polyQ–expressing neurons.

To qualify as a toxic mediator, the function and/or abundance of Relish should be up-regulated by toxic MJD polyQ proteins. Thus, we first examined whether the molecular function of Relish as a TF is up-regulated by toxic MJD polyQ proteins in fly brain. To this end, we compared mRNA expression levels of well-known Relish target genes (*CecA1*, *CecA2*, *CecB*, *AttA*, *AttB*, and *DptB*; De Gregorio et al., 2002; Tanji et al., 2010) between control fly heads and those panneuronally expressing MJD-78Q. The mRNA levels of all target genes examined were significantly increased by MJD-78Q (Fig. 1 E), indicating that the molecular function of Relish is up-regulated by MJD-78Q. We then examined whether the amount of Relish is increased by MJD-78Q as well. For this, through Western blot analysis, we compared the amounts of endogenous Relish between control fly heads and those panneuronally expressing MJD-78Q. The amount of endogenous Relish was significantly ($P < 0.05$) increased in brains expressing MJD-78Q compared with control brains (Fig. 1, F and G). Taken together, these data suggest that Relish is a novel toxic mediator of polyQ-induced dendrite defects.

PolyQ-induced dendrite defects require Dredd-mediated endoproteolytic cleavage of Relish to generate N-terminal fragment of Relish, Rel68

Next, we questioned how Relish abnormally gains the toxicity that contributes to dendrite defects induced by the expression of MJD polyQ proteins. To address this, we first examined whether overexpression of Relish has toxic effects on dendrite morphology. Unexpectedly, overexpression of Relish in C4da neurons did not show noticeable changes in dendrite morphology, determined by the number of branch points and dendritic complexity (Fig. 2, A and B; and Fig. S2 A). Because endoproteolytic cleavage of Relish by Dredd (a *Drosophila* homologue of Caspase-8) is known to be required for activation of its TF

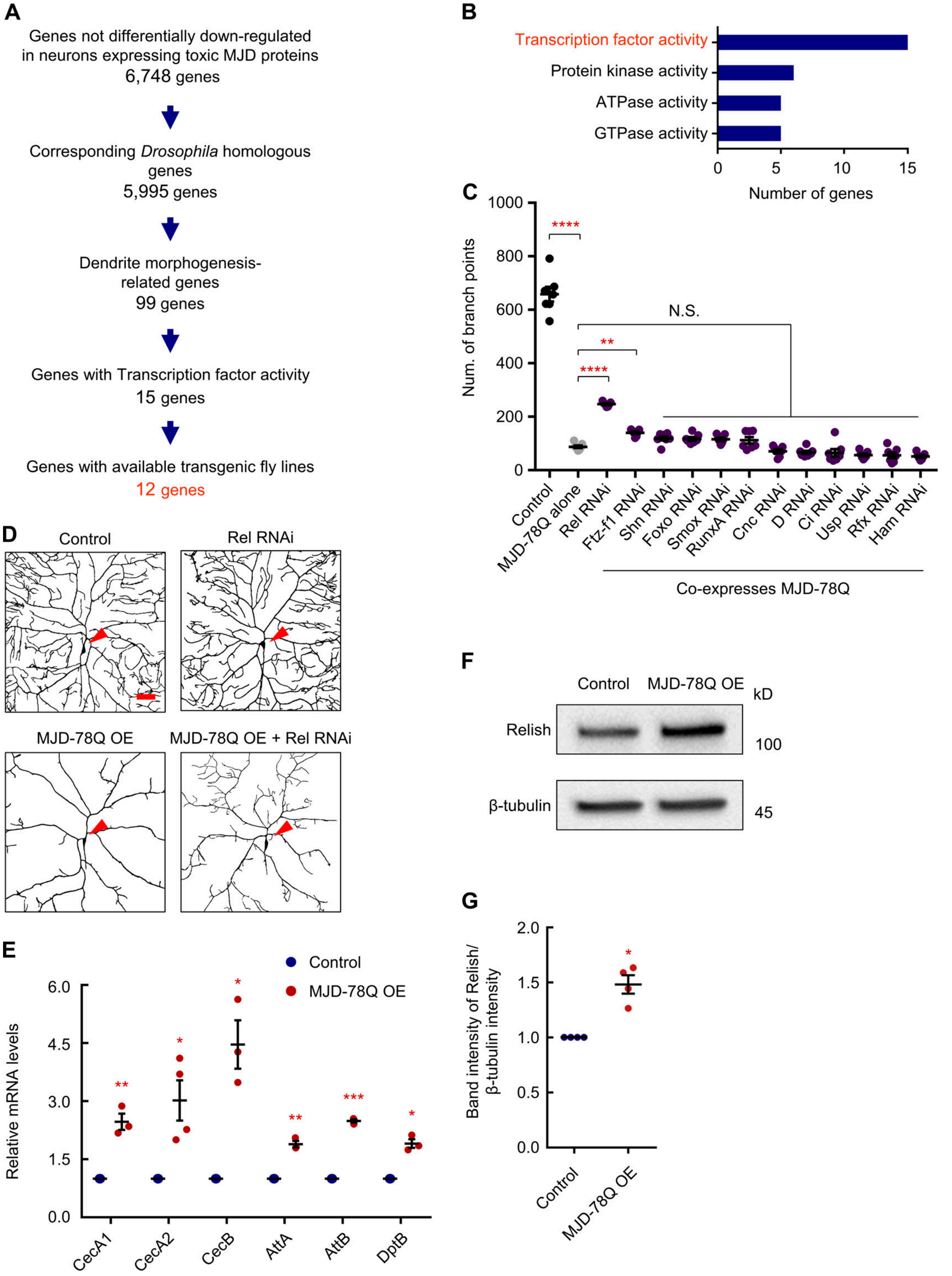

Figure 1. **Identification of Relish as a novel toxic mediator of MJD polyQ–induced dendrite defects. (A)** Overall scheme for selection of candidates for toxic mediators of MJD polyQ–induced dendrite defects. **(B)** The GOMFs enriched in selected 99 genes related to dendrite morphogenesis. Gene ontology analysis was done using DAVID. Among GOMF terms, we selected terms representing functionality of proteins, such as TF activity, but not terms representing interaction property of proteins, such as binding activities and dimerization activities. **(C)** Quantification of the number of dendrite branch points of control C4da neurons and C4da neurons expressing MJD-78Q alone or MJD-78Q + denoted RNAi transgenes. For comparison between control C4da neurons and C4da neurons expressing MJD-78Q alone, Student's *t* test was used; ****, $P < 1.0 \times 10^{-4}$; error bars, SEM; *n* = 7 neurons. For comparison between C4da neurons expressing MJD-78Q alone and those coexpressing MJD-78Q + denoted transgenes, one-way ANOVA was used with Tukey post hoc test; N.S., not significant; **, $P < 1.0 \times 10^{-2}$; ****, $P < 1.0 \times 10^{-4}$; error bars, SEM; *n* = 7 neurons. **(D)** Representative images of control C4da neuron (upper left) and C4da neurons expressing Relish RNAi (upper right), MJD-78Q (lower left) or co-overexpressing MJD-78Q + Relish RNAi (lower right). (*UAS-CD4tdGFP/+;ppk-gal4/+*, *UAS-CD4tdGFP/+;ppk-gal4/UAS-Rel RNAi* [BL33661], *UAS-CD4tdGFP/+;ppk-gal4,UAS-MJD-78Q/+*, and *UAS-CD4tdGFP/+;ppk-gal4,UAS-MJD-78Q/UAS-Rel RNAi* [BL33661]). Red-colored arrowheads indicate cell bodies of C4da neurons. Scale bar, 50 µm. **(E)** Quantification of band intensities of RT-PCR products reflecting mRNA levels of

transcriptional target genes of Relish (*CecA1*, *CecA2*, *CecB*, *AttA*, *AttB*, and *DptB*) in control fly heads and those expressing MJD-78Q (*elav-gal4*/+ and *UAS-MJD-78Q*/+;*elav-gal4*/+). *, $P < 0.05$; **, $P < 1.0 \times 10^{-2}$; ***, $P < 1.0 \times 10^{-3}$ by Student's *t* test; error bars, SEM; *n* = 3 independent experiments. **(F)** Representative images of Western blot analysis using whole cell lysates of adult fly heads (*elav-gal4*/+ and *UAS-MJD-78Q*/+;*elav-gal4*/+). Full-length form of endogenous Relish was detected using anti-Relish-C antibody (21F3), and β-tubulin (E7) was used as a loading control. **(G)** Quantification of band intensities in F reflecting amounts of endogenous Relish. The quantified band intensity of Relish was normalized by that of β-tubulin in each sample. *, $P < 0.05$ by Student's *t* test; error bars, SEM; *n* = 4 independent experiments.

function (Stöven et al., 2000; Fig. S2 B), we then examined whether cleaved fragments of Relish have toxic effects on dendrite morphology. N-terminal (Rel68) and C-terminal (Rel49) fragments of Relish, generated by endoproteolytic cleavage, contain Relish homology domain with TF activity and an ankyrin repeat domain, respectively (Fig. S2 C; Stöven et al., 2000). Overexpression of Rel68 in C4da neurons significantly ($P < 1.0 \times 10^{-4}$) reduced both the number of dendrite branch points and dendritic complexity compared with control, whereas overexpression of Rel49 did not induce noticeable change in dendrite morphology (Fig. 2, A and B; and Fig. S2 A). These data indicate that Rel68, but not Rel49 nor uncleaved Relish, has toxicity inducing changes in dendrite morphology in C4da neurons.

Next, we wondered whether polyQ-induced dendrite defects involve endoproteolytic cleavage of Relish to generate Rel68. To address this, we attempted to examine whether toxic MJD polyQ proteins change the quantity of these two protein fragments through Western blot analysis. However, neither fragment was detected by commercially available Rel49 antibody or our newly generated antibody for Rel68 (not depicted). We instead turned to genetic analysis to determine whether Dredd-mediated endoproteolytic cleavage of Relish to generate Rel68 contributes to polyQ-induced dendrite defects. To this end, we knocked down Dredd in C4da neurons expressing MJD-78Q and compared the consequent dendrite phenotypes to those caused by expression of MJD-78Q alone. Knockdown of Dredd significantly ($P < 1.0 \times 10^{-4}$) suppressed polyQ-induced dendrite defects (Fig. 2, C and D), while knockdown of Dredd only in C4da neurons did not induce noticeable changes in dendrite morphology and dendrite branch points (Fig. S2, D and E). Consistently, overexpression of Caspar, an upstream inhibitor of Dredd (Fig. S2 B), significantly restored polyQ-induced dendrite defects in C4da neurons (Fig. 2, C and D), while overexpression of Caspar only in C4da neurons did not induce noticeable changes in dendrite morphology and dendrite branch points (Fig. S2, D and E). In addition, we found that knockdown of Dredd or Caspar overexpression did not induce significant changes in the amount of MJD-78Q proteins (Fig. S3, A–F), suggesting that the restoration effect of Dredd RNAi or Caspar overexpression does not result from reduced amounts of toxic MJD polyQ proteins. These data suggest that Dredd-mediated endoproteolytic cleavage of Relish contributes to polyQ-induced dendrite defects.

Then, we asked how toxic MJD polyQ proteins affect Dredd-mediated endoproteolytic cleavage of Relish. We first checked whether Dredd mRNA levels were up-regulated by expression of MJD polyQ proteins and found that Dredd mRNA was not up-regulated in the existing RNA-sequencing database (Chung et al., 2017). Given that toxic polyQ proteins have a high propensity to sequester their target molecules, resulting in their loss of function (Chung et al., 2017; Kwon et al., 2018), the toxic polyQ proteins may up-regulate Dredd activity by aberrantly interacting with an upstream negative regulator of Dredd, such as Caspar. A search for known negative regulators of Dredd, other than Caspar, revealed none, so we hypothesized that toxic MJD polyQ proteins may aberrantly interact with Caspar in neurons. To explore this, we overexpressed Caspar in C4da neurons, with or without MJD-78Q expression, and compared localization patterns of Caspar. Overexpressed Caspar alone in C4da neurons showed dispersed localization throughout the cytoplasm, with relatively scarce localization in the nucleus (Figs. 2 E and S3 G). By contrast, overexpression of Caspar in C4da neurons expressing MJD-78Q showed aberrant localization in the nucleus, with puncta formation that colocalized with MJD-78Q (Figs. 2 E and S3 G), supporting our hypothesis of aberrant interaction between Caspar and MJD polyQ proteins. To confirm this aberrant interaction, we performed a coimmunoprecipitation experiment in HEK293T cells expressing Caspar with or without MJD-76Q and found that Caspar was coimmunoprecipitated with MJD-76Q (Fig. 2 F). Collectively, these data suggest that disinhibition of Relish toxicity required for polyQ-induced dendrite defects results from up-regulation of Dredd-mediated endoproteolytic cleavage of Relish to generate Rel68 owing to aberrant interactions between Caspar and toxic MJD polyQ proteins.

Increased nuclear localization of N-terminal fragment of Relish is required for polyQ-induced dendrite defects

Then, to further support that N-terminal fragment of Relish contributes to polyQ-induced dendrite defects, we searched for characteristic molecular features of Rel68 that are distinct from full-length Relish and Rel49. According to previous studies, Rel68 translocates from the cytoplasm to the nucleus to act as a TF (Wiklund et al., 2009). Thus, we examined subcellular localization of Relish and its cleaved fragments in C4da neurons. We found that only Rel68, but not Relish nor Rel49, preferentially localized in the nucleus of C4da neurons (Fig. S4, A and B). In addition, we found that Rel68, but not Rel49, transcriptionally regulates the expression of downstream targets of Relish (*CecA1*, *CecA2*, *CecB*, *AttB*, and *DptB*) in fly brain by performing RT-PCR experiments (Fig. 3 A). Based on these findings showing that Rel68, but not Rel49, predominantly localizes to the nucleus to function as a TF in neurons, we hypothesized that nuclear localization of Rel68 is critical for MJD-78Q–induced dendrite defects. Next, we examined whether MJD-78Q expression increases the nuclear localization of Relish. Because of the lack of antibodies detecting N-terminal fragment of endogenous Relish, we co-overexpressed dual-tagged full-length Relish (Flag-Relish-V5) and MJD-78Q in C4da neurons and detected N-terminus

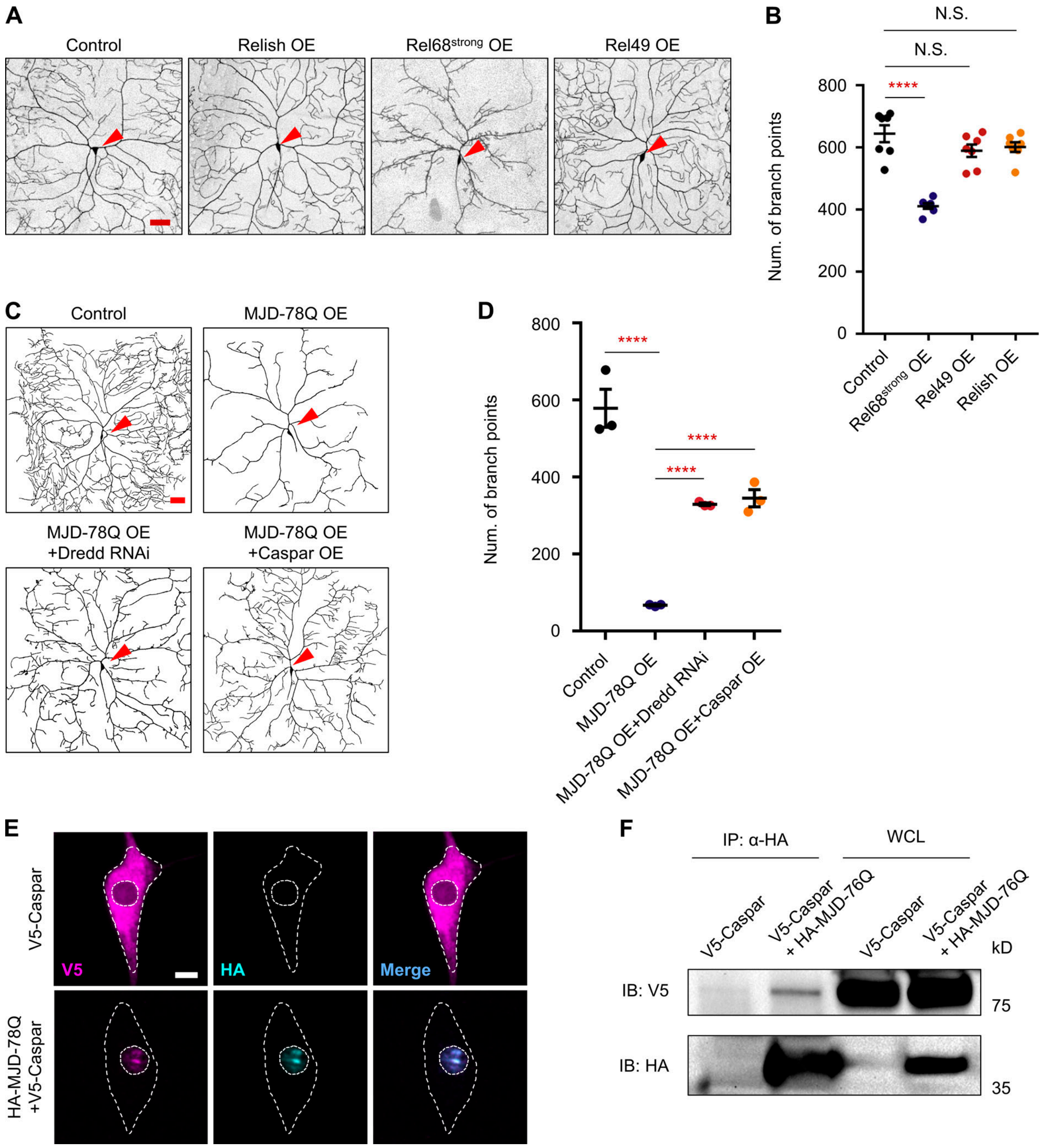
A
Control
Relish OE
Rel68strong OE
Rel49 OE
B
N.S.
N.S.
****
Num. of branch points
800
600
400
200
0
Control
Rel68strong OE
Rel49 OE
Relish OE
C
Control
MJD-78Q OE
MJD-78Q OE +Dredd RNAi
MJD-78Q OE +Caspar OE
D
****
****
****
Num. of branch points
800
600
400
200
0
Control
MJD-78Q OE
MJD-78Q OE+Dredd RNAi
MJD-78Q OE+Caspar OE
E
V5-Caspar
HA-MJD-78Q +V5-Caspar
V5
HA
Merge
F
IP: α-HA
WCL
V5-Caspar
V5-Caspar + HA-MJD-76Q
V5-Caspar
V5-Caspar + HA-MJD-76Q
kD
IB: V5
75
IB: HA
35

Figure 2. **Restoration of polyQ-induced dendrite defects by reduced endoproteolytic cleavage of Relish to generate N-terminal fragment of Relish, Rel68. (A)** Representative images of control C4da neuron (leftmost panel) and C4da neurons overexpressing Relish (second from left), Rel68^{strong} (third from left), or Rel49 (rightmost panel). (*UAS-CD4tdGFP/+;ppk-gal4/+*, *UAS-CD4tdGFP/+;ppk-gal4/UAS-Rel-3xHA*, *UAS-Flag-Rel68/+;UAS-CD4tdGFP/+;ppk-gal4/+*, and *UAS-CD4tdGFP/UAS-Rel-V5.49;ppk-gal4/+*). Red-colored arrowheads indicate cell bodies of C4da neurons. Scale bar, 50 µm. **(B)** Quantification of the number of dendrite branch points of C4da neurons overexpressing denoted transgenes in A. N.S., not significant; ****, $P < 1.0 \times 10^{-4}$ by one-way ANOVA with Tukey post hoc test; error bars, SEM; *n* = 7 neurons. **(C)** Representative images of control C4da neuron (upper left) and C4da neurons expressing MJD-78Q (upper right), co-overexpressing MJD-78Q + Dredd RNAi (lower left), or co-overexpressing MJD-78Q + Caspar (lower right). (*UAS-CD4tdGFP/+;ppk-gal4/+*, *UAS-CD4tdGFP/+;ppk-gal4,UAS-MJD-78Q/+*, *UAS-CD4tdGFP/+;ppk-gal4,UAS-MJD-78Q/UAS-Dredd RNAi*, and *UAS-CD4tdGFP/UAS-2xV5-Caspar;ppk-gal4,UAS-MJD-78Q/+*). Red-colored arrowheads indicate cell bodies of C4da neurons. Scale bar, 50 µm. **(D)** Quantification of the number of dendrite branch points of C4da neurons expressing denoted transgenes in C. For comparison of the number of dendrite branch points between control C4da neurons and those expressing MJD-78Q alone, Student's *t* test was used; ****, $P < 1.0 \times 10^{-4}$; error bars, SEM; *n* = 3 neurons. For the comparison among C4da neurons expressing MJD-78Q, MJD-78Q + Dredd RNAi, and MJD-78Q + Caspar, one-way ANOVA was used with Tukey post hoc test; ****, $P < 1.0 \times 10^{-4}$; error bars, SEM; *n* = 3 neurons. **(E)** Subcellular localization of V5-Caspar (magenta) and HA-MJD-78Q (cyan) in C4da neurons expressing V5-Caspar or co-overexpressing V5-Caspar + HA-MJD-78Q (*UAS-CD4tdGFP/UAS-2xV5-Caspar;ppk-gal4/+* and *UAS-CD4tdGFP/UAS-2xV5-Caspar;ppk-gal4,UAS-HA-MJD-78Q/+*). Overexpressed V5-Caspar and HA-MJD-78Q were detected using anti-V5 and anti-HA antibodies, respectively. Outer and inner dashed lines (white) indicate outlines of cell body and nucleus, respectively. Scale bar, 5 µm. **(F)** Representative images of Western blot analysis using protein lysates immunoprecipitated (IP) with α-HA antibody and whole-cell lysates (WCL) using HEK293T cells transfected with *2xV5-Caspar* or *2xV5-Caspar + 2xHA-MJD-76Q*. *n* = 3 independent experiments. IB, immunoblot.

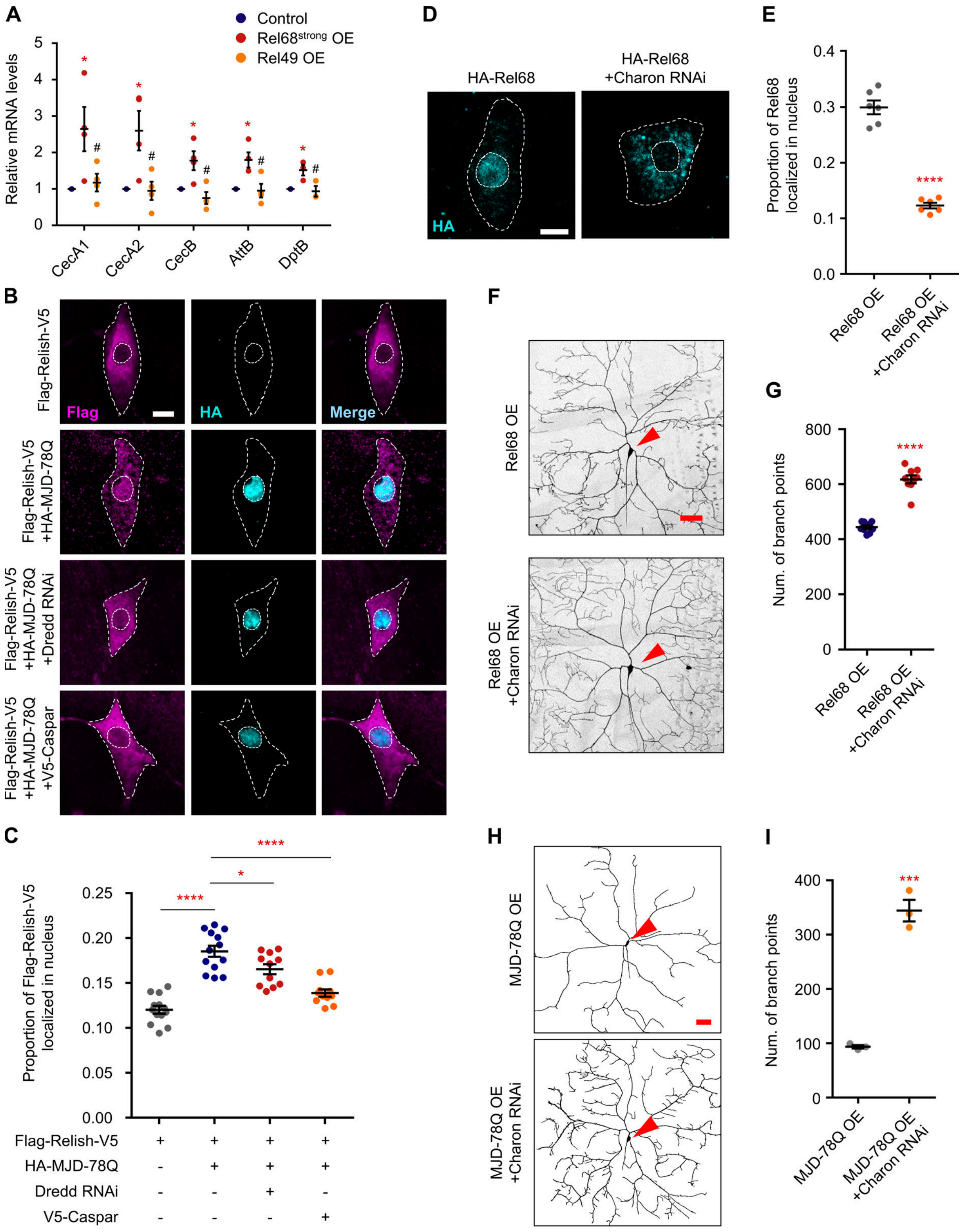

Figure 3. **Contribution of increased nuclear localization of N-terminal fragment of Relish to polyQ-induced dendrite defects. (A)** Quantification of band intensities of RT-PCR products reflecting mRNA levels of Relish downstream genes (*CecA1*, *CecA2*, *CecB*, *AttB*, and *DptB*) in control fly heads and those expressing Rel68^{strong} or Rel49 (*elav-gal4/+*, *UAS-Flag-Rel68/+;;elav-gal4/+*, and *UAS-Rel49-V5/+;elav-gal4/+*). #, not significant; *, $P < 0.05$ by one-way ANOVA with Tukey post hoc test; error bars, SEM; $n = 3$ independent experiments. **(B)** Representative distribution patterns of Flag-Relish-V5 (detected using anti-Flag antibody) in C4da neurons expressing denoted genes. Subcellular localization of MJD-78Q proteins was detected by anti-HA antibody (*UAS-2xFlag-Relish-2xV5/UAS-CD4tdGFP;ppk-gal4/+*, *UAS-2xFlag-Relish-2xV5/UAS-CD4tdGFP;ppk-gal4,UAS-HA-MJD-78Q/+*, *UAS-2xFlag-Relish-2xV5/UAS-CD4tdGFP;ppk-gal4,UAS-HA-MJD-78Q/UAS-Dredd RNAi*, and *UAS-2xFlag-Relish-2xV5/UAS-2xV5-Caspar;ppk-gal4,UAS-HA-MJD-78Q/+*). Outer and inner dashed lines (white) indicate outlines of cell body and nucleus, respectively. Scale bar, 5 µm. **(C)** Quantification of nuclear proportion of Flag-positive Relish in C4da neurons expressing denoted gene in B.

For comparison of nuclear proportion of Flag-positive Relish between C4da neurons expressing Flag-Relish-V5 and those co-overexpressing Flag-Relish-V5 and MJD-78Q, Student's *t* test was used; ****, $P < 1.0 \times 10^{-4}$; error bars, SEM. For comparison of nuclear proportion of Flag-positive Relish among C4da neurons expressing Flag-Relish-V5+MJD-78Q, Flag-Relish-V5+MJD-78Q+Dredd RNAi, and Flag-Relish-V5+MJD-78Q+Caspar, one-way ANOVA was used with Tukey post hoc test; *, $P < 0.05$; ****, $P < 1.0 \times 10^{-4}$; error bars, SEM. The number of neurons tested are as follows: Flag-Relish-V5 = 13, Flag-Relish-V5+MJD-78Q = 13, Flag-Relish-V5+MJD-78Q+Dredd RNAi = 11, and Flag-Relish-V5+MJD-78Q+Caspar = 11. **(D)** Subcellular localization of Rel68 in C4da neurons expressing Rel68 (left) or co-overexpressing Rel68 + Charon RNAi (right). (*UAS-2xHA-Rel68/+;ppk*^{1a}*-gal4,UAS-CD4tdGFP/+* and *UAS-2xHA-Rel68/UAS-Charon RNAi;ppk*^{1a}*-gal4,UAS-CD4tdGFP/+*). Overexpressed Rel68 was detected using anti-HA antibody. Outer and inner dashed lines (white) indicate outlines of cell body and nucleus, respectively. Scale bar, 5 µm. **(E)** Quantification of nuclear proportion of Rel68 in C4da neurons expressing denoted transgenes in D. ****, $P < 1.0 \times 10^{-4}$ by Student's *t* test; error bars, SEM; $n = 6$ neurons. **(F)** Representative dendrite images of C4da neurons overexpressing Rel68 (upper) or co-overexpressing Rel68 + Charon RNAi (lower). (*UAS-Flag-Rel68/+;ppk*^{1a}*-gal4,UAS-CD4tdGFP/+* and *UAS-Flag-Rel68/UAS-Charon RNAi;ppk*^{1a}*-gal4,UAS-CD4tdGFP/+*). Red-colored arrowheads indicate cell bodies of C4da neurons. Scale bar, 50 µm. **(G)** Quantification of the number of dendrite branch points in C4da neuron expressing transgenes described in F. ****, $P < 1.0 \times 10^{-4}$ by Student's *t* test; error bars, SEM; $n = 9$ neurons. **(H)** Representative dendrite images of C4da neurons expressing MJD-78Q (upper) or co-overexpressing MJD-78Q + Charon RNAi (lower). (*UAS-CD4tdGFP/+;ppk-gal4,UAS-MJD-78Q/+* and *UAS-CD4tdGFP/UAS-Charon RNAi;ppk-gal4,UAS-MJD-78Q/+*). Red-colored arrowheads indicate cell bodies of C4da neurons. Scale bar, 50 µm. **(I)** Quantification of the number of dendrite branch points in C4da neuron expressing denoted transgenes in H. ***, $P < 1.0 \times 10^{-3}$ by Student's *t* test; error bars, SEM; $n = 3$ neurons.

of Relish using anti-Flag antibody. Of note, both cleaved and full-length forms of Relish are detected by anti-Flag immunostaining. Consequently, overexpression of MJD-78Q resulted in significantly increased nuclear proportions of Relish proteins detected by anti-Flag antibody (Flag-positive Relish) in C4da neurons; however, this increase in nuclear localization of Flag-positive Relish was markedly decreased by coexpression of Dredd RNAi or Caspar (Fig. 3, B and C). Together with our above results, that dendrite defects caused by toxic polyQ proteins were significantly restored by coexpression of Dredd RNAi or Caspar (Fig. 2, C and D) and that Caspar proteins aberrantly interact with toxic polyQ proteins (Fig. 2, E and F), these data suggest that nuclear localization of N-terminal fragment of Relish is increased by polyQ toxicity owing to aberrant up-regulation of Relish cleavage pathway, thereby resulting in dendrite defects.

Next, we further investigated whether inhibition of nuclear localization of Rel68 ameliorates polyQ-induced dendrite defects. To address this, we prevented nuclear localization of Rel68 in C4da neurons by knockdown of Charon mediating nuclear localization of Rel68 (Ji et al., 2016) and confirmed that Charon knockdown markedly reduced the nuclear localization of Rel68 (Fig. 3, D and E). Then, we examined whether the inhibition of nuclear localization of Rel68 by Charon knockdown suppresses Rel68-induced dendrite defects. To this end, we compared dendrite morphology of C4da neurons overexpressing both Charon RNAi and Rel68 with that of C4da neurons overexpressing Rel68 alone. Notably, the Rel68-induced decrease in number of dendrite branch points was significantly ($P < 1.0 \times 10^{-4}$) restored by Charon knockdown (Fig. 3, F and G), indicating that the nuclear localization of Rel68 is required for Rel68-induced neuronal toxicity causing dendrite defects. Next, we examined whether nuclear localization of Rel68 is required for polyQ-induced dendrite defects as well. PolyQ-induced dendrite defects were also significantly ($P < 1.0 \times 10^{-3}$) ameliorated by knockdown of Charon in C4da neurons (Fig. 3, H and I). In addition, we confirmed that inhibition of nuclear localization of Rel68 resulted in decreased mRNA expression of Relish target genes (Fig. S4 C) up-regulated by MJD-78Q (Fig. 1 E). Taken together, these data suggest that increased nucleus-localized N-terminal fragment of Relish contributes to dendrite defects induced by toxic polyQ proteins.

Newly identified transcriptional target genes of Rel68, *Tup* and *Pros*, mediate Rel68 toxicity contributing to dendrite defects induced by MJD-78Q

We then wondered what transcriptional target genes of Rel68 mediate Rel68-induced dendritic toxicity. Target genes of Relish or NF-κB identified in previous studies have broad molecular functions, but are primarily associated with immune response, such as cytokines and immunoreceptors (Cao et al., 2006; Hinz et al., 2001; Hiscott et al., 1993). To identify novel Rel68 target genes involved in Rel68-induced dendritic toxicity, we selected candidates from 171 *Drosophila* proteins whose functions are dendrite morphogenesis based on gene ontology biological process annotation, and further 51 TFs among them, since transcriptional regulation is the most strongly associated with dendrite morphogenesis (Fig. 1 B). To determine whether 41 of 51 TFs with mammalian homologues available are transcriptional target genes of Rel68, we used RT-PCR analysis to compare their mRNA levels in adult fly heads panneuronally overexpressing Rel68 with those in control heads (Fig. 4 A). Among the 41 TFs, we found 8 genes up-regulated ($\log_2$ fold-changes ≥ 0.4, 1.3-fold) by Rel68 overexpression (*Prospero* [*Pros*], *Cut* [*Ct*], *Abnormal chemosensory jump 6* [*Acj6*], *Pox meso* [*Poxm*], *Enhancer of Polycomb* [*E*[*Pc*]], *Hamlet* [*Ham*], *Tailup* [*Tup*], and *Sequoia* [*Seq*]), as well as three genes down-regulated ($\log_2$ fold changes ≤ −0.4) by Rel68 overexpression (*Hand*, *Absent*, *small*, or *homeotic discs* 2 [*Ash2*], and *Domino* [*Dom*]). These data raise a possibility that these dendrite morphology–associated genes may be novel transcriptional target genes of Rel68 and mediate Rel68-induced neuronal toxicity causing dendrite defects.

Using available fly lines, we first confirmed the roles of transcriptionally up-regulated or down-regulated target genes of Rel68 in dendrite morphogenesis by examining dendrite phenotypes of C4da neurons with their increased or decreased gene expression, respectively. Among eight transcriptionally up-regulated genes, five (*Pros*, *Ct*, *Poxm*, *Tup*, and *Seq*) were available for overexpression transgenes, whose overexpression all markedly reduced the number of dendrite branch points in C4da neurons (Fig. 4 B). For three transcriptionally down-regulated genes, knockdown of each of Dom, Hand, and Ash2 in C4da neurons caused significant ($P < 1.0 \times 10^{-3}$) reduction in the number of dendrite branch points (Fig. 4 B). Then, we examined whether Rel68-induced dendrite phenotypes can be

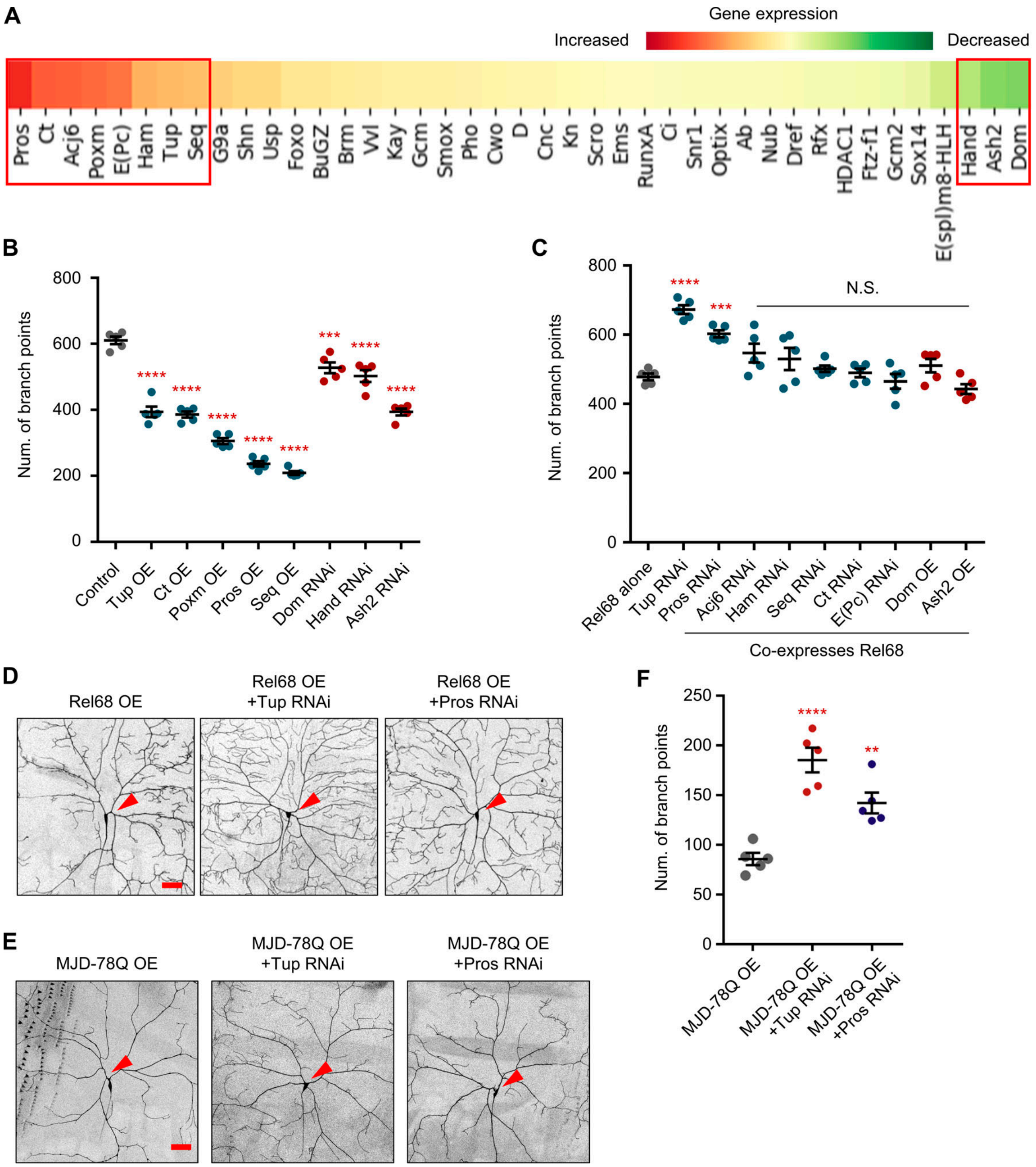

Figure 4. **Identification of *Tup* and *Pros* as novel transcriptional target genes of Rel68 contributing to Rel68-induced dendrite defects. (A)** Heatmap showing increased (red) or decreased (green) mRNA levels of TFs regulating dendrite morphogenesis in adult fly heads expressing Rel68 compared with control heads (*elav-gal4/+* and *UAS-Flag-Rel68/+;;elav-gal4/+*). Genes showing absolute $\log_2$ fold-changes >0.4 are indicated using the red boxes. *n* = 3 independent experiments. **(B)** Quantification of the number of dendrite branch points in control C4da neurons and C4da neurons expressing denoted transgenes driven by *ppk*^{1a}*-gal4*. Genes identified to be transcriptionally up-regulated or down-regulated by Rel68 in A are marked with teal or red colors, respectively. ***, $P < 1.0 \times 10^{-3}$; ****, $P < 1.0 \times 10^{-4}$ by one-way ANOVA with Tukey post hoc test; error bars, SEM; *n* = 5 neurons. **(C)** Quantification of the number of dendrite branch points in C4da neurons expressing Rel68 alone or Rel68 + denoted transgenes driven by *ppk*^{1a}*-gal4*. Genes identified to be transcriptionally up-regulated or down-regulated by Rel68 in A are marked with teal or red colors, respectively. N.S., not significant; ***, $P < 1.0 \times 10^{-3}$; ****, $P < 1.0 \times 10^{-4}$ by one-way ANOVA with Tukey post hoc test; error bars, SEM; *n* = 5 neurons. **(D)** Representative dendrite images of C4da neurons expressing Rel68, Rel68 + Tup RNAi, or Rel68 + Pros RNAi (*UAS-Flag-Rel68/+;ppk*^{1a}*-gal4,UAS-CD4tdGFP/+*, *UAS-Flag-Rel68/+;ppk*^{1a}*-gal4,UAS-CD4tdGFP/UAS-Tup RNAi*, and *UAS-Flag-Rel68/UAS-Pros RNAi;ppk*^{1a}*-gal4,UAS-CD4tdGFP/+*). Red-colored arrowheads indicate cell bodies of C4da neurons. Scale bar, 50 µm. **(E)** Representative dendrite images of C4da neurons expressing MJD-78Q, MJD-78Q + Tup RNAi, or MJD-78Q + Pros RNAi (*UAS-CD4tdGFP/+;ppk-gal4,UAS-MJD-78Q/+*, *UAS-CD4tdGFP/+;ppk-gal4,UAS-MJD-78Q/UAS-Tup RNAi*, and *UAS-CD4tdGFP/UAS-Pros RNAi;ppk-gal4,UAS-MJD-78Q/+*). Red-colored arrowheads indicate cell bodies of C4da neurons. Scale bar, 50 µm. **(F)** Quantification of the number of dendrite branch points in C4da neuron expressing denoted transgenes in E. **, $P < 1.0 \times 10^{-2}$; ****, $P < 1.0 \times 10^{-4}$ by one-way ANOVA with Tukey post hoc test; error bars, SEM; *n* = 5 neurons.

restored by decreasing or increasing expression levels of transcriptionally up-regulated or down-regulated target genes, respectively. Among seven transcriptionally up-regulated genes tested, only knockdown of Tup and Pros in C4da neurons showed significant restoration of Rel68-induced dendrite phenotypes (Fig. 4, C and D). On the other hand, overexpression of two transcriptionally down-regulated genes tested (*Dom* and *Ash2*) did not significantly restore Rel68-induced dendrite phenotypes (Fig. 4 C). These data suggest *Tup* and *Pros* as novel transcriptional target genes of Rel68 that mediate Rel68-induced dendritic toxicity. Then, we wondered whether Tup and Pros are key downstream effectors of Rel68 toxicity that contribute to polyQ-induced dendrite defects. To address this, we knocked down Tup or Pros in C4da neurons expressing MJD-78Q and examined dendrite phenotypes. Knockdown of Tup or Pros significantly ($P < 1.0 \times 10^{-2}$) restored dendrite defects caused by MJD-78Q expression in C4da neurons (Fig. 4, E and F). Collectively, these data demonstrate that Tup and Pros are novel downstream effectors of Rel68 that mediate Rel68 toxicity and contribute to toxic polyQ-induced dendrite defects.

To examine whether Rel68 directly regulates the expression of Tup and Pros, we performed chromatin immunoprecipitation (ChIP)-PCR analysis to assess binding enrichment of Rel68 to promoter regions of *Tup* and *Pros* in fly heads panneuronally overexpressing Rel68. ChIP-PCR analysis showed significant enrichment of Rel68 in promoter regions of *Tup* (Fig. S5 A) and *Pros* (Fig. S5 B). These data collectively suggest that Rel68 directly binds to the promoters of *Tup* and *Pros* to up-regulate their expression and induces dendrite defects.

Rel68-induced neuronal cell death and behavioral abnormalities are mediated by Tup

Having characterized Relish-induced dendrite defects in the context of MJD polyQ disease and identified Tup and Pros as downstream mediators, we next wondered whether Rel68 induces additional neuronal toxicity beyond dendrite defects, and if so, whether Tup or Pros is associated with these toxicities as well. Of note, overexpression of a strong allele of Rel68 ($\mathrm{Rel68^{strong}}$) in C4da neurons frequently resulted in complete loss of dendrites and axon tract, indicative of neurodegeneration (Fig. 5, A and B). This observation is consistent with a previous study showing degenerative eye phenotypes caused by Rel68 overexpression in *Drosophila* (Chinchore et al., 2012). The ratio of degenerating C4da neurons by $\mathrm{Rel68^{strong}}$ overexpression was significantly ($P < 0.05$) reduced by knockdown of Tup or Pros (Fig. 5 B).

We next examined whether overexpression of Rel68 in dendritic arborization (da) neuronal clusters can lead to organism-level changes in larval motility assessed by measuring crawling and head-turning activities (Riedl and Louis, 2012). We first tested the crawling activity determined by the time for the larvae to reach the dish edge, as previously described (Kwon et al., 2018), using the following four different lines of larvae: control larvae and larvae expressing Rel68, Tup, or Rel68 + Tup RNAi in da neuronal clusters using the *109(2)80*-Gal4 driver. All control larvae reached the edge of the dish within 100 s, whereas only 26.6% of larvae overexpressing Rel68 reached the edge in this time (Fig. 5, C and D). The fraction of larvae expressing Rel68 reaching the edge of the dish increased significantly from 26.6% to 57.6% when Tup was knocked down (Fig. 5, C and D). Of note, only 16.4% of larvae overexpressing Tup reached the edge of the dish, comparable to the value of larvae overexpressing Rel68 (Fig. 5, C and D), supporting that Tup mediates Rel68-induced behavioral defects. To measure head-turning activity, we monitored the changes in angle of a larval head for 1 min, as previously described (Kwon et al., 2018). Control larvae barely turned their heads (Fig. 5, E and F), whereas larvae overexpressing Rel68 turned their heads frequently (Fig. 5, E and F). The frequent head turning of larvae expressing Rel68 was significantly reduced by knockdown of Tup (Fig. 5, E and F). Larvae overexpressing Tup showed frequent head turning, comparable to larvae overexpressing Rel68 (Fig. 5, E and F), which is consistent with observations on crawling activity described above. Collectively, these data demonstrate that Rel68-induced neuronal cell death and behavioral abnormalities are mediated by Tup.

Rel68-mediated neuronal toxicity contributes to dendrite and behavioral defects in animal models for ALS

We next wondered whether Rel68-mediated neuronal toxicity contributes to neuropathic features of NDs other than polyQ diseases. To address this, we used the *C9orf72*-associated ALS (C9ALS) fly model expressing an expanded GGGGCC 30-repeat $(\mathrm{G4C2})_{30}$ (Xu et al., 2013) to induce dendrite (Burguete et al., 2015) and behavioral (Goodman et al., 2019; Xu et al., 2013) defects and examined whether knockdown of Relish or Tup can suppress these defects. First, we checked whether overexpression of $(\mathrm{G4C2})_{30}$ up-regulates TF activity of Relish by measuring mRNA levels of transcriptional target genes of Relish (*CecA1*, *CecA2*, *CecB*, *AttA*, *AttB*, and *DptB*) in adult fly heads. Overexpression of $(\mathrm{G4C2})_{30}$ significantly increased mRNA levels of all tested target genes (Fig. 6 A). Furthermore, as shown in C4da neurons expressing MJD-78Q (Fig. 3, B and C), significantly increased nuclear localization of Flag-positive Relish was observed in C4da neurons expressing $(\mathrm{G4C2})_{30}$ (Fig. S6, A and B). Collectively, these data suggest the increased TF activity of Relish due to the increase in nuclear localization of N-terminal fragment of Relish in the C9ALS model.

We then examined whether knockdown of Relish or Tup can suppress dendrite defects induced by $(\mathrm{G4C2})_{30}$. Overexpression of $(\mathrm{G4C2})_{30}$ in C4da neurons significantly reduced the number of dendrite branch points (Fig. 6, B and C) as previously reported (Burguete et al., 2015). These dendrite defects were significantly suppressed by knockdown of Relish or Tup (Fig. 6, B and C). In addition, we further tested whether G4C2 repeat expansion–mediated dendrite defects can be synergistically aggravated by Rel68. The reduced number of dendrite branch points by Rel68 or $(\mathrm{G4C2})_{30}$ overexpression was significantly aggravated by co-overexpression of $(\mathrm{G4C2})_{30}$ and Rel68 (Fig. 6, D and E). These data demonstrate that the Rel68-Tup pathway mediates the dendrite defects of C9ALS model as well. Next, we performed a negative geotaxis assay to compare climbing activity among control adult flies and adult flies panneuronally expressing $(\mathrm{G4C2})_{30}$, $(\mathrm{G4C2})_{30}$ + Relish RNAi, or $(\mathrm{G4C2})_{30}$ + Tup RNAi. Flies overexpressing $(\mathrm{G4C2})_{30}$ showed significantly reduced climbing

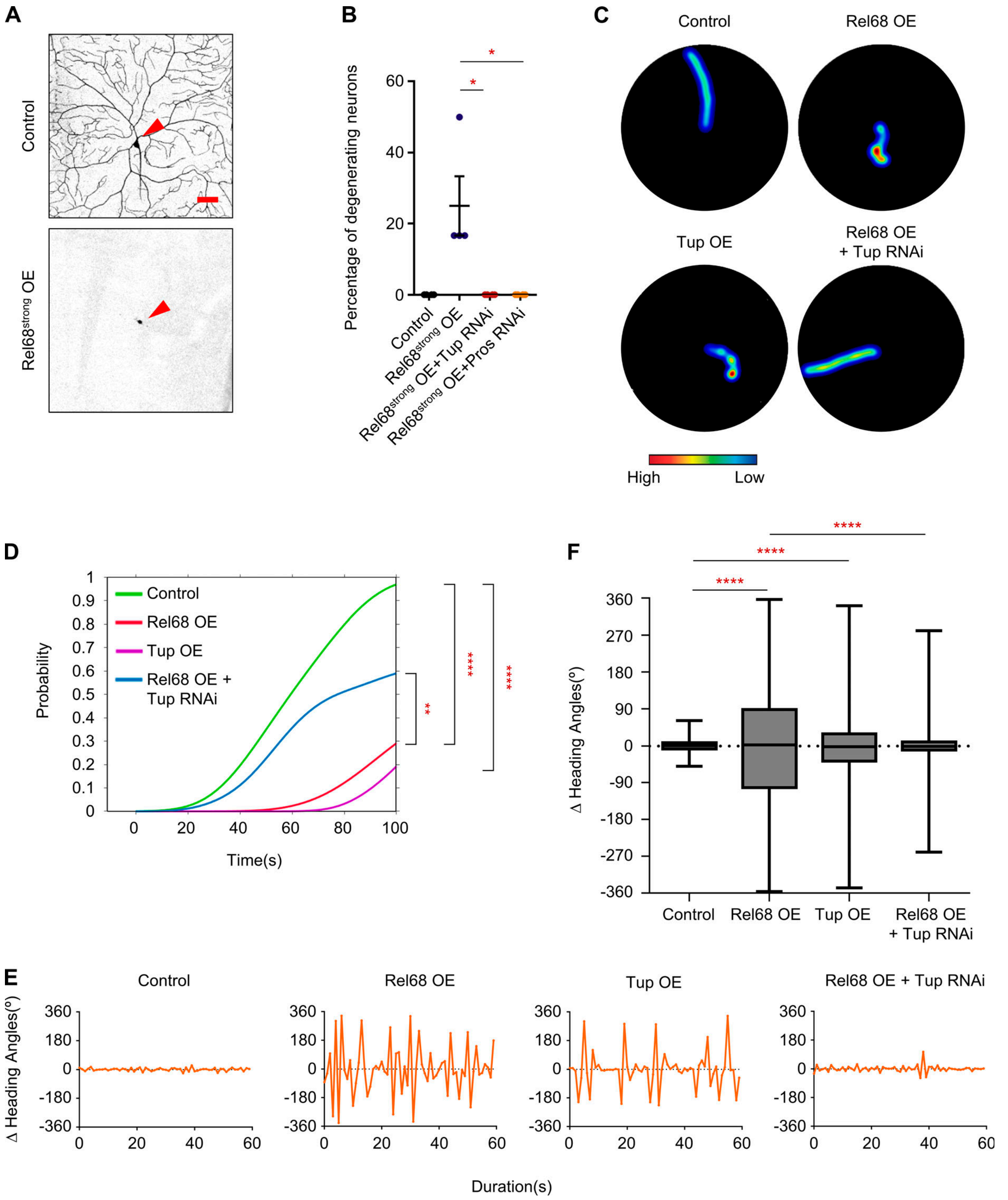

Figure 5. **Rel68-induced neuronal cell death and behavioral abnormalities mediated by Tup. (A)** Representative image of C4da neuron showing neurodegeneration by overexpression of Rel68^{strong} (lower) and that of control C4da neuron (upper). (*ppk^{1a}-gal4,UAS-CD4tdGFP/+* and *UAS-Flag-Rel68/+;;ppk^{1a}-gal4,UAS-CD4tdGFP/+*). Red-colored arrowheads indicate cell bodies of C4da neurons. Scale bar, 50 µm. **(B)** Percentage of degenerating C4da neurons expressing denoted transgenes. *, $P < 0.05$ by one-way ANOVA with Tukey post hoc test; error bars, SEM; $n = 4$ larvae. **(C)** Representative heatmap images showing residence probability during traveling of larvae expressing denoted transgenes for 100 s (*109(2)80-gal4/+*, *109(2)80-gal4,UAS-Flag-Rel68/+*, *109(2)80-gal4/UAS-Tup*, and *109(2)80-gal4,UAS-Flag-Rel68/+;UAS-Tup RNAi/+*). **(D)** Cumulative density functions showing proportion of larvae that reached the edge of Petri dish over time. The functions are estimated separately for larvae expressing each of the transgenes described in C. **, $P < 1.0 \times 10^{-2}$; ****, $P < 1.0 \times 10^{-4}$ by random permutation experiments. The numbers of larvae tested are as follows: Control = 26, Tup = 20, Rel68 = 25, and Rel68 + Tup RNAi = 29. **(E)** Representative changing patterns of head angles of larvae, taken every second for 1 min. Turning the head to left and right is presented as positive (+) and negative (−), respectively. The patterns are obtained separately for larvae expressing each of the transgenes described in C. **(F)** Box plots showing the variability of head angle changes in larvae expressing the transgenes described in C. ****, $P < 1.0 \times 10^{-4}$ by random permutation experiments; $n = 4$ independent larvae.

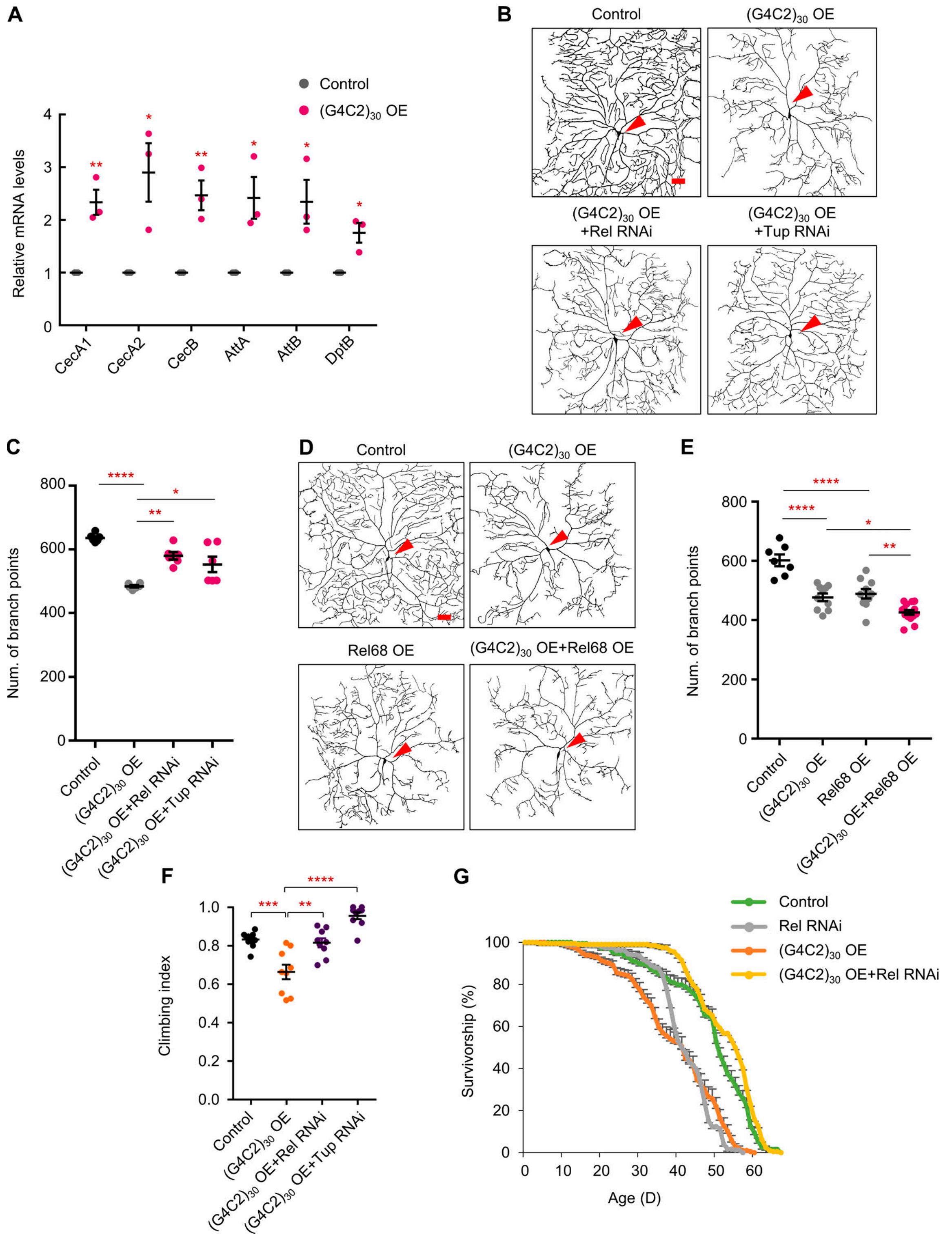

Figure 6. **Contribution of Rel68 to dendrite and behavioral defects in C9ALS model. (A)** Quantification of band intensities of RT-PCR products reflecting mRNA levels of transcriptional target genes of Relish (*CecA1*, *CecA2*, *CecB*, *AttA*, *AttB*, and *DptB*) in control fly brains and those expressing $(G4C2)_{30}$ (*elav-gal4/+* and *UAS-*$(G4C2)_{30}$*/+;elav-gal4/+*). *, $P < 0.05$; **, $P < 1.0 \times 10^{-2}$ by Student's *t* test; error bars, SEM; *n* = 3 independent experiments. **(B)** Representative dendrite images of control C4da neuron and C4da neurons expressing $(G4C2)_{30}$, $(G4C2)_{30}$ + Relish RNAi, or $(G4C2)_{30}$ + Tup RNAi (ppk^{1a}*-gal4,UAS-CD4tdGFP/+*, *UAS-*$(G4C2)_{30}$*/+;*ppk^{1a}*-gal4,UAS-CD4tdGFP/+*, *UAS-*$(G4C2)_{30}$*/+;*ppk^{1a}*-gal4,UAS-CD4tdGFP/UAS-Rel RNAi* [BL33661], and *UAS-*$(G4C2)_{30}$*/+;*ppk^{1a}*-gal4,UAS-CD4tdGFP/UAS-Tup RNAi*). Red-colored arrowheads indicate cell bodies of C4da neurons. Scale bar, 50 µm. **(C)** Quantification of the number of branch points of C4da neurons expressing denoted transgenes in B. For comparison of the number of dendrite branch points between control C4da neurons and those expressing $(G4C2)_{30}$, Student's *t* test was used; ****, $P < 1.0 \times 10^{-4}$; error bars, SEM; *n* = 6 neurons. For comparison among C4da neurons expressing $(G4C2)_{30}$, $(G4C2)_{30}$ + Relish RNAi, and $(G4C2)_{30}$ + Tup RNAi, one-way ANOVA was used with Tukey post hoc test; *, $P < 0.05$; **, $P < 1.0 \times 10^{-2}$; error bars, SEM; *n* = 6 neurons. **(D)** Representative dendrite images of control C4da neuron and those expressing $(G4C2)_{30}$, Rel68, or $(G4C2)_{30}$ + Rel68 (ppk^{1a}*-gal4,UAS-CD4tdGFP/+*,

UAS-(G4C2)$_{30}$*/+;ppk*^{1a}*-gal4,UAS-CD4tdGFP/+*, *UAS-Flag-Rel68/+;ppk*^{1a}*-gal4,UAS-CD4tdGFP/+*, and *UAS-Flag-Rel68/UAS-(G4C2)*$_{30}$*;ppk*^{1a}*-gal4,UAS-CD4tdGFP/+*). Red-colored arrowheads indicate cell bodies of C4da neurons. Scale bar, 50 µm. **(E)** Quantification of the number of branch points of C4da neurons expressing denoted transgenes in D. *, $P < 0.05$; **, $P < 1.0 \times 10^{-2}$; ****, $P < 1.0 \times 10^{-4}$ by two-way ANOVA with Tukey post hoc test; error bars, SEM. The number of neurons tested are as follows: Control = 7, (G4C2)$_{30}$ = 10, Rel68 = 10, and (G4C2)$_{30}$ + Rel68 = 14. **(F)** Quantification of climbing ability in control adult flies and adult flies panneuronally expressing (G4C2)$_{30}$, (G4C2)$_{30}$ + Relish RNAi, and (G4C2)$_{30}$ + Tup RNAi at 3 d after eclosion (*elav-gal4/+*, *UAS-(G4C2)*$_{30}$*/+;elav-gal4/+*, *UAS-(G4C2)*$_{30}$*/+;elav-gal4/UAS-Rel RNAi* [BL33661], and *UAS-(G4C2)*$_{30}$*/+;elav-gal4/UAS-Tup RNAi*). Climbing index indicates proportion of flies that climbed >10 cm within 10 s. For the comparison of climbing index between control flies and flies panneuronally expressing (G4C2)$_{30}$, Student's *t* test was used; ***, $P < 1.0 \times 10^{-3}$; error bars, SEM. For comparison of climbing index among flies panneuronally expressing (G4C2)$_{30}$, (G4C2)$_{30}$ + Relish RNAi, and (G4C2)$_{30}$ + Tup RNAi, one-way ANOVA was used with Tukey post hoc test; **, $P < 1.0 \times 10^{-2}$; ****, $P < 1.0 \times 10^{-4}$; error bars, SEM. The numbers of flies tested are as follows: Control = 120, (G4C2)$_{30}$ = 125, (G4C2)$_{30}$ + Relish RNAi = 112, and (G4C2)$_{30}$ + Tup RNAi = 105. **(G)** Comparison of survival rates over time among control flies and flies panneuronally expressing Relish RNAi, (G4C2)$_{30}$, and (G4C2)$_{30}$ + Relish RNAi (*elav-gal4/+*, *elav-gal4/UAS-Rel RNAi* [BL33661], *UAS-(G4C2)*$_{30}$*/+;elav-gal4/+*, and *UAS-(G4C2)*$_{30}$*/+;elav-gal4/UAS-Rel RNAi* [BL33661]). The numbers of flies tested are as follows: Control = 192, Relish RNAi = 184, (G4C2)$_{30}$ = 194, and (G4C2)$_{30}$ + Relish RNAi = 197.

activity compared with control flies (Fig. 6 F), consistent with previous reports (Goodman et al., 2019). The reduced climbing activity was significantly ($P < 1.0 \times 10^{-2}$) restored by knockdown of Relish or Tup (Fig. 6 F). Furthermore, we also assessed the lifespan of control flies and flies panneuronally overexpressing (G4C2)$_{30}$ or (G4C2)$_{30}$ + Relish RNAi (Fig. 6 G). Flies overexpressing (G4C2)$_{30}$ showed reduced lifespan compared with control flies, consistent with previous studies (Mizielinska et al., 2014; Moens et al., 2019). Knockdown of Relish in flies overexpressing (G4C2)$_{30}$ suppressed the G4C2 repeat expansion–mediated reduction in lifespan, while knockdown of Relish in control flies showed reduced lifespan (Fig. 6 G; Discussion). Taken together, these data demonstrate that Rel68-mediated neuronal toxicity contributes to dendrite and behavioral defects in the C9ALS model.

Discussion

In this study, we identified disinhibition of latent Relish toxicity as a novel pathogenic mechanism of action underlying dendrite and behavioral defects in animal models for two NDs, MJD polyQ disease and C9ALS. Our data showed that, as a mechanism mediating disinhibition of Relish toxicity in MJD polyQ disease condition, Dredd-mediated endoproteolytic cleavage of Relish to generate N-terminal fragment of Relish was up-regulated by aberrant interaction between Caspar and MJD toxic polyQ proteins (Fig. 2, E and F; and Fig. 3, B and C). This is further supported by our observation that overexpression of Relish alone in C4da neurons did not induce dendrite phenotypes (Fig. 2 A), indicating that increased abundance of Relish may be not a key determinant of neuronal toxicity associated with dendrite defects. As for C9ALS condition, based on the following previous studies, we speculate that up-regulation of Dredd-mediated endoproteolytic cleavage of Relish is similarly applicable as well. Although the cleavage-based regulation of NF-κB in mammals is different from that of Relish in *Drosophila*, Caspase-8 and Dredd share a conserved function of activating NF-κB and Relish, respectively. Previous studies showed that Caspase-8, a mammalian homologue of Dredd, is up-regulated in patient samples of ALS, potentially by loss of function of optineurin that binds to Caspase-8 (Nakazawa et al., 2016), and that genetic mutations in optineurin have been observed in patients with ALS (Maruyama et al., 2010). It will be valuable to see whether documented changes in subcellular localization, activity, and intracellular expression level of NF-κB seen in ND neurons and/or glial cells (Table S1) are, in fact, associated with our proposed pathogenic model involving disinhibition of latent NF-κB toxicity.

NF-κB plays various well-characterized essential physiological roles, including regulation of immune response (Cao et al., 2006; Hinz et al., 2001; Hiscott et al., 1993) and cell death (Chinchore et al., 2012). In the nervous system, the most recognized role involves regulation of neuroinflammation in glial cells, such as microglia and astrocytes (Shih et al., 2015). Aberrant activation of neuroinflammation is often observed in the late stages of various NDs, which leads to nonselective degeneration of neurons throughout the entire brain. The dysregulation of NF-κB, therefore, has garnered great attention since it was reported that NF-κB contributes to non–cell-autonomous neurodegeneration in late stages of NDs (Heneka et al., 2015; Hirsch and Hunot, 2009; Philips and Robberecht, 2011). In contrast, in this study, we characterized, for the first time, cell-autonomous effects of NF-κB on an early pathogenic feature, dendrite defects, in animal models for NDs.

The up-regulation of quantity and/or activity of NF-κB has been consistently seen in neurons of both ND patients and animal models for ND (Table S1), supporting our finding of cell-autonomous contribution of NF-κB in neurons to the disease pathogenesis. Consistently, several previous studies showed that NF-κB induces neuronal toxicity in a cell-autonomous manner. Among five mammalian homologues of Relish, RelA/p65 is known to confer neuronal toxicity, inducing ectopic cell death by forming a heterodimer with p50 in ischemic conditions (Sarnico et al., 2009). In addition, knockdown of RelA reduced glutamate-mediated cell death of cerebellar granule neurons, which is indicative of a neuronal proapoptotic function of RelA (Pizzi et al., 2002). Likewise, overexpression of Rel68 in *Drosophila* eyes induced degenerative phenotypes (Chinchore et al., 2012). Interestingly, however, a neuroprotective role of NF-κB in a cell-autonomous manner has been also proposed. For example, Bhakar et al. (2002) showed that overexpression of RelA prevented cell death of primary cortical neurons induced by neurotoxins such as camptothecin and etoposide. In addition, overexpression of RelA can promote cellular survival of cultured nodose neurons (Gutierrez et al., 2005). Consistently, we observed that panneuronal expression of Relish RNAi alone reduced lifespan compared with the control (Fig. 6 G). Therefore, based on these findings, functional roles of NF-κB in neurons could be shifted between protective and toxic depending on the cellular and environmental context, and amounts and functions of NF-κB in neurons should be tightly regulated to sustain neuronal homeostasis and health. Future studies elucidating specific functions and modes of regulation of NF-κB in various cellular environmental contexts are expected to broaden our understanding of the basic principles of neuronal maintenance and pathophysiology of neurological disorders associated with NF-κB.

The main mechanism proposed in this study is the aberrant increase in the nucleus-localized N-terminal fragment of Relish by changes in cleavage machinery due to the toxic disease proteins. Even though this mechanism is supported by our genetic and immunohistochemical results (Fig. 2, C–F; and Fig. 3, B–I), Western blot analysis directly detecting N-terminal fragment of Relish is thought to be the most direct evidence related to this. However, when we performed Western blot analysis to detect N-terminal fragment of Relish using anti-Flag antibody, which detects N-terminus of dual-tagged full-length Relish (Flag-Relish-V5), for unknown reasons, it failed to detect any signals of cleaved N-terminal fragment of Relish. Consistent with our results, a previous study in *Drosophila* cell line reported that Flag-tagged N-terminal fragment of Relish is barely detected through Western blot analysis (Tanji et al., 2010). Alternatively, we showed the involvement of cleavage machinery of Relish on the nuclear localization of Flag-positive Relish in C4da neurons using immunohistochemistry accompanied by genetic modulation of cleavage machinery (Fig. 3, B and C). We expect that further studies surely can overcome this technical limitation and provide solid evidence supporting the conclusion of this study.

In this study, we present clear evidence for NF-κB–induced neuronal toxicity in the context of NDs. We also identified Tup and Pros as mediators of NF-κB–induced neuronal toxicity. Given that our findings propose therapeutic measures to intervene in polyQ disease and C9ALS before significant dendrite defects occur, we speculate that inhibitor-based therapeutics targeting Relish/NF-κB and/or downstream mediators (Tup and Pros) may be of particular use in modifying NDs, especially during early stages of disease.

Materials and methods

Fly stocks

Following fly stocks were obtained from Bloomington Drosophila Stock Center: *UAS-Pros.L* (BL32244), *UAS-Tup* (BL39661), *UAS-Rel RNAi* (BL33661), *UAS-Dredd RNAi* (BL34070), *UAS-Pros RNAi* (BL42538), *UAS-Tup RNAi* (BL51763), *UAS-Shn RNAi* (BL34689), *UAS-Ftz-f1 RNAi* (BL33625), *UAS-Ci RNAi* (BL64928), *UAS-Smox RNAi* (BL41670), *UAS-Rfx RNAi* (BL61847), *UAS-RunxA RNAi* (BL33353), *UAS-D RNAi* (BL34672), *UAS-Foxo RNAi* (BL32427), *UAS-Cnc RNAi* (BL32863), *UAS-Usp RNAi* (BL56729), *UAS-Seq.B* (BL9244), *UAS-Dom RNAi* (BL38385), *UAS-Seq RNAi* (BL51923), *UAS-Ct RNAi* (BL29625), *UAS-E(Pc) RNAi* (BL67921), *UAS-Dom.A* (BL64262), *UAS-MJD-78Q* (BL8150), *UAS-MJD-78Q* (BL8141), *elav-gal4* (BL8760), *UAS-Rel-V5.49* (BL55779), *UAS-Flag-Rel.68* (BL55777), and *UAS-Flag-Rel.68* (BL55778). *UAS-Flag-Rel.68* (BL55777) has higher expression levels of Rel68 and therefore is denoted as Rel68^{strong} in this study. *UAS-Flag-Rel68* (BL55778) has milder expression levels of Rel68 and is denoted as Rel68 in this study. *UAS-Rel RNAi* (KK108469), *UAS-Rel RNAi* (GD49413), *UAS-Charon RNAi* (KK106292), *UAS-Hand RNAi* (GD23306), *UAS-Ash2 RNAi* (GD7141), *UAS-Ham RNAi* (GD40763), and *UAS-Acj6 RNAi* (KK105292) were obtained from Vienna Drosophila Resource Center. The following fly lines were obtained from Fly ORF: *UAS-Rel-3xHA* (F001780), *UAS-Poxm* (F003333), and *UAS-Ash2-3xHA* (F003904). *UAS-(GGGGCC)$_{30}$* was kindly provided by Peng Jin (Emory University School of Medicine, Atlanta, GA). *Hsp70*-Gal4 was kindly provided by Y.N. Jan (University of California San Francisco, San Francisco, CA). The following lines were used as previously described (Kwon et al., 2018): *ppk-gal4* (III), *ppk^{1a}-gal4* (III), *109(2)80-gal4* (II), *UAS-CD4tdGFP* (II), and *UAS-CD4tdGFP* (III). All fly stocks were raised at room temperature (25°C) with 60% humidity except for negative geotaxis assay and lifespan assay (temperature, 27°C; humidity, 60%).

Generation of transgenic fly lines

Following transgenic fly lines were generated in this study: *UAS-2xFlag-Relish-2xV5*, *UAS-2xHA-Rel68*, and *UAS-2xV5-Caspar*. The transgene of *UAS-2xFlag-Relish-2xV5* was synthesized by Biomatik. *UAS-2xHA-Rel68* transgene was generated by engineering the *UAS-2xFlag-Relish-2xV5* transgene. The *UAS-2xV5-Caspar* transgene was generated using LD03368 clone (Berkeley *Drosophila* Genome Project). All transgenes were incorporated into pACU2 vector, and each transgenic fly line was generated by BestGene.

Immunohistochemistry

Third instar larval fillet was fixed with 3.7% formaldehyde for 20 min at room temperature. After brief washing with 0.3% PBT (PBS containing 0.3% Triton X-100), dissected tissues were incubated in blocking buffer (5% normal donkey serum in 0.3% PBT) for 50 min at room temperature. The tissues were incubated at 4°C with primary antibody. The following primary antibodies were used in this study: rat anti-HA (3F10, Roche; 1:200 dilution) for detecting the HA epitope; mouse anti-V5 (R960-25; Thermo Fisher Scientific; 1:200) for detecting the V5 epitope; and mouse anti-Flag (1E6, Wako; 1:200) for detecting the Flag epitope. To detect primary antibodies, the following secondary antibodies were used: donkey anti-mouse cy3 (Jackson Immunoresearch Laboratories; 1:300), goat anti-mouse Alexa Fluor 647 (Invitrogen; 1:1,000), goat anti-HRP Alexa Fluor 488 (Jackson Immunoresearch Laboratories; 1:1,000), and goat anti-rat Alexa Fluor 647 (Jackson Immunoresearch Laboratories; 1:1,000).

Confocal image acquisition

All confocal images of C4da neurons were obtained from abdominal segments A4 and A5 using LSM700, LSM780, or LSM800 microscopes (Zeiss) at 20°C. For live imaging of C4da neurons genetically labeled with mCD4tdGFP, an individual third-instar larva was mounted in 1× PBS, and C4da neurons were captured using a 20×/0.5-NA objective. For imaging of immunostained samples, a larval fillet was mounted in PBG (70% glycerol in 1× PBS), and C4da neurons were captured using a 40×

water/2.0-NA objective. The following fluorochromes were used in immunostaining experiments: Alexa Fluor 488, Alexa Fluor 647, cy3, and EGFP. After image acquisition, maximum-intensity projections of each image were obtained using Zeiss Zen software, and additional image processing (pseudocolor filters or deconvolution) was applied in Adobe Photoshop CC.

Western blot analysis and coimmunoprecipitation

Western blot analysis was performed as previously described (Kwon et al., 2018). Protein lysates were extracted from adult fly heads using lysis buffer (150 mM NaCl, 1% Triton X-100, and 50 mM Tris-HCl, pH 7.5). Next, 4× Laemmli sample buffer (161-0747; Bio-Rad) and β-mercaptoethanol were mixed with 30 µg of total proteins of each extracted sample to be 1× and 2.5%, respectively. The mixture was incubated for 5 min at 95°C and loaded into Mini-PROTEAN TGX Stain-Free, 4–15% gel (BR456-8083; Bio-Rad) for electrophoresis. The separated proteins were transferred to the nitrocellulose membrane (BR170-4270; Bio-Rad), and the nitrocellulose membrane was incubated in blocking buffer (TBST [50 mM Tris-HCl, pH 7.4, 150 mM NaCl, and 0.1% Tween-20] containing 5% skim milk) for 1 h at room temperature. To detect endogenous Relish and β-tubulin, mouse anti-Relish-C (21F3; Developmental Studies Hybridoma Bank; 1:1,000) and mouse anti-β-tubulin (E7; Developmental Studies Hybridoma Bank; 1:1,000) were used, respectively. For detecting HA-MJD-78Q protein, rat anti-HA (3F10; Roche; 1:1,000) antibody was used. To detect primary antibodies, the following secondary antibodies were used: anti-mouse IgGκ BP HRP conjugated (sc-516102; Santa Cruz; 1:3,000) and goat anti-rat IgG-HRP (sc-2006; Santa Cruz; 1:3,000).

To identify protein interactions between MJD-76Q and Caspar through coimmunoprecipitation, HEK293T cells were transfected with *2xV5-Caspar* and *2xHA-MJD-76Q* subcloned into EGFP-N1 vector and cultured for 24 h before sample preparation. Harvested HEK293T cells were homogenized in lysis buffer (150 mM NaCl, 1% Triton X-100, and 50 mM Tris-HCl, pH 7.5), and whole-cell lysates containing equivalent protein amounts were incubated with 1 µg of rat anti-HA (3F10; Roche) at 4°C overnight. After the incubation, the precleaned protein A/G plus agarose beads (sc-2003; Santa Cruz) with lysis buffer were coincubated with the whole-cell lysates containing HA antibody for 3 h at 4°C in a shaking incubator. After the incubation, the beads were washed with lysis buffer three times, and immunoprecipitated proteins were eluted in 1× Laemmli sample buffer containing 2.5% β-mercaptoethanol. These immunoprecipitated proteins were separated through electrophoresis and transferred to nitrocellulose membrane as described above. To detect Caspar and MJD-76Q through Western blot analysis, mouse anti-V5 (R960-25; Thermo Fisher Scientific; 1:1,000) and rat anti-HA (3F10; Roche; 1:1,000) antibodies were used, respectively. To detect primary antibodies, the following secondary antibodies were used: anti-mouse IgGκ BP HRP conjugated (sc-516102; Santa Cruz; 1:3,000) and goat anti-rat IgG-HRP (sc-2006; Santa Cruz; 1:3,000).

RT-PCR

RT-PCR analysis was performed as previously described (Chung et al., 2017). Total RNAs were extracted from adult fly heads using Easy-Blue system (iNtRON Biotechnology). cDNAs were synthesized from 3 µg of total RNAs using GoScript Reverse Transcription (A2791; Promega) according to the manufacturer's standard protocol. For RT-PCR analysis, each target gene was amplified with the corresponding primer set (Table S2 and Table S3) using GoTaq G2 Master Mixes (M7823; Promega) in a C1000 Thermal Cycler, C1000 Touch Thermal Cycler, or T100 Thermal Cycler system (Bio-Rad).

ChIP-PCR

Because of the lack of available ChIP-grade antibody that specifically precipitates endogenous Rel68, we panneuronally overexpressed HA-Rel68 and examined whether overexpressed HA-Rel68 is enriched in the promoter regions of *Tup* or *Pros*. ChIP-PCR experiments were performed as previously described (Chung et al., 2017). First, fly heads were collected in ice-cold 1× PBS. After elimination of the PBS, the collected fly heads were homogenized in fixation buffer (1.5% formaldehyde, 0.143 M NaCl, 1.43 mM EDTA, 71.45 mM Hepes-KOH, pH 7.5, and 1× protease inhibitor [87786; Thermo Fisher Scientific]) and incubated for 20 min at room temperature to cross-link target TFs with chromatin. Then, glycine and Tris were added to the fixation buffer to be 370 mM and 2.5 mM, respectively, and incubated for 5 min at room temperature to terminate the cross-linking reaction. After 5-min centrifugation at 4,000 *g*, the pellet was washed with Tris-buffered saline (20 mM Tris-HCL, pH 7.5, and 150 mM NaCl), FA lysis buffer (50 mM Hepes-KOH, pH 7.5, 150 mM NaCl, 1 mM EDTA, 1% Triton X-100, 0.1% SDS, and 0.1% Na-deoxycholate), FA lysis buffer/0.5% SDS (50 mM Hepes-KOH, pH 7.5, 150 mM NaCl, 1 mM EDTA, 1% Triton X-100, 0.5% SDS, and 0.1% Na-deoxycholate), and FA lysis buffer sequentially. The pellet was then resuspended in FA lysis buffer.

For the chromatin shearing, the resuspended sample was sonicated for 20 min using Covaris M220 with following conditions: peak power, 70.0; duty factor, 25.0; cycles/burst, 200; average power, 17.5. The sheared nucleosomes were acquired after centrifugation for 10 min at 17,000 *g*. After Bradford assay, input control was prepared from the lysates, and remaining lysates were incubated with 3 µg of anti-HA antibody (C29F4; Cell Signaling Technology) at 4°C overnight. Next, precleaned protein A/G plus agarose beads (sc-2003; Santa Cruz) with FA lysis buffer were added into the lysates containing HA antibody and incubated for 4 h at 4°C. The beads were precipitated and washed with FA lysis buffer and washing buffer (10 mM Tris-HCl, pH 8.0, 0.25 M LiCl, 1 mM EDTA, 0.5% NP-40, and 0.5% Na-deoxycholate) sequentially. Sheared chromatin precipitated with the beads were eluted using elution buffer (50 mM Tris-HCl, pH 7.5, 10 mM EDTA, and 1% SDS) at 65°C for 20 min. The eluted samples and prepared input control were incubated with RNase (1 mg/ml) at 37°C for 1 h. After 42°C incubation with proteinase K (20 mg/ml) for 1 h, the samples were incubated at 65°C for 5 h. The DNA was then extracted using phenol-chloroform-isoamyl alcohol.

Next, quantitative PCR (qPCR) experiments were performed using the extracted DNA with QuantiSpeed SYBR Green kit (QS105-10; PhilKorea) and CFX96 TouchTM Real-Time PCR Detection System (Bio-Rad). For PCR amplification of samples, the following primers were used: Tup promoter, forward 5′-AGTTCGACAAGCGCATTACAACAG-3′ and reverse 5′-TGCCAATTTCGCTTTTGGTTTTCG-3′; Tup ORF, forward 5′-GGCATGACTCCCCACTGAATCT-3′ and reverse 5′-GTGTGGGTATTGATCGCTCCATT-3′; Pros promoter, forward 5′-CCTTTTTGGACCGCGCTTCATT-3′ and reverse 5′-CCCCCTCCGTATGTAAAAGCATCT-3′; Pros ORF, forward 5′-CCCCAGAATTTCCGCTTCGT-3′ and reverse 5′-CGACTTGAAGTACTCGGGCAC-3′.

Larval motility assay and data processing

The larval motility assay was performed as previously described (Kwon et al., 2018). *109(2)80*-gal4 driver was used to express each transgene in da neuronal clusters. Each larva was washed in 1× PBS and placed in the center of a 90-mm Petri dish. The motility assay was performed inside a dark box with indirect lighting. After 1-min acclimation, we recorded total elapsed time for larvae to reach the edge of a 90-mm Petri dish up to 100 s. Then, we estimated a cumulative density function by using the Gaussian kernel density estimation method (Bowman and Azzalini, 1997) and evaluated statistical significance of difference between the cumulative density function of each genotype using Matlab.

To analyze larval motility from acquired video files, we used EthoVision XT (v11.5; Noldus Information Technology) video tracking system. In Fig. 5 C, the entire trace of larva was converted into a heatmap in which color represents elapsed time that larva spent in the specific location. For all heatmaps, the amount of time was normalized to those during 100 s. For head-turning behavior of larva, we used the *Heading* tool in EthoVision XT and calculated changes in head angle of each larva every second for 1 min. We evaluated the statistical significance of the difference in head-turning angles of each genotype using Matlab.

Negative geotaxis assay

Right after eclosion from pupa, 15 flies of each genotype were collected and reared for 3 d at 27°C with 60% humidity. After 3 d, these flies were transferred to an acrylic cylinder closed at one end (3-cm diameter, 18-cm height) without CO_2 anesthesia, and the top of the cylinder was sealed with sponges to block escape. After 30-min acclimation at room temperature, the flies were placed on the bottom of the cylinder by tapping the cylinder five times against a table, and climbing was recorded for 1 min. Climbing ability was measured with a climbing index (proportion of 15 flies climbing >10 cm from the bottom of cylinder within 10 s) in each experimental group of flies.

Statistical analysis

Statistical analysis was performed using Prism 7 (GraphPad Software) with Student's unpaired *t* test, one-way ANOVA (with Tukey post hoc test), or two-way ANOVA (with Tukey post hoc test). Data distribution was assumed to be normal, but this was not formally tested. Values are presented as mean ± SEM. $P < 0.05$ was considered statistically significant (*, $P < 0.05$; **, $P < 1.0 \times 10^{-2}$; ***, $P < 1.0 \times 10^{-3}$; and ****, $P < 1.0 \times 10^{-4}$).

Online supplemental material

Fig. S1 shows that the restoration effects of Relish RNAi on polyQ-induced dendrite defects are not attributed to the changes in the amount of MJD-78Q proteins. Fig. S2 shows that knockdown and overexpression of the regulators of endoproteolytic cleavage of Relish (Dredd and Caspar, respectively) have no effect on dendrite morphology. Fig. S3 shows that the restoration effects of Dredd knockdown or Caspar overexpression on polyQ-induced dendrite defects are not attributed to the changes in the amount of MJD-78Q proteins. Fig. S4 supports Fig. 3 by showing that the increased transcriptional activity of Relish by toxic polyQ proteins is significantly reduced by the inhibition of its nuclear localization by Charon RNAi. Fig. S5 shows enrichment of Rel68 in the promoters of *Tup* and *Pros*. Fig. S6 shows increased nuclear proportion of Flag-positive Relish in C4da neurons co-overexpressing $(G4C2)_{30}$ and dual-tagged full-length Relish (Flag-Relish-V5). Table S1 lists studies reporting association of NF-κB with NDs and aging. Table S2 and Table S3 include detailed information about primers used for RT-PCR.

Acknowledgments

This work was supported by Basic Science Research Program through the National Research Foundation of Korea, funded by the Ministry of Science and ICT, South Korea (2018R1A2B6001607 and 2019R1A4A1024278 to S.B. Lee); the Development of Platform Technology for Innovative Medical Measurements Program from the Korea Research Institute of Standards and Science (KRISS-2019-GP2019-0018 to S.B. Lee); and Korea Brain Research Institute basic research program, funded by Ministry of Science and ICT, South Korea (20-BR-04-02 to S.B. Lee).

The authors declare no competing financial interests.

Author contributions: M.H. Han, M.J. Kwon, B.S. Ko, and S.B. Lee conceived the project. M.H. Han, M.J. Kwon, B.S. Ko, D.Y. Hyeon, and D. Hwang performed experiments and analyzed the data. M.H. Han, M.J. Kwon, B.S. Ko, D. Lee, H.-J. Kim, and S.B. Lee interpreted the data and wrote the manuscript.

Submitted: 16 April 2020
Revised: 18 August 2020
Accepted: 5 October 2020

References

Adler, A.S., S. Sinha, T.L. Kawahara, J.Y. Zhang, E. Segal, and H.Y. Chang. 2007. Motif module map reveals enforcement of aging by continual NF-kappaB activity. *Genes Dev.* 21:3244–3257. https://doi.org/10.1101/gad.1588507

Bhakar, A.L., L.L. Tannis, C. Zeindler, M.P. Russo, C. Jobin, D.S. Park, S. MacPherson, and P.A. Barker. 2002. Constitutive nuclear factor-kappa B activity is required for central neuron survival. *J. Neurosci.* 22:8466–8475. https://doi.org/10.1523/JNEUROSCI.22-19-08466.2002

Blumenstock, S., E.F. Rodrigues, F. Peters, L. Blazquez-Llorca, F. Schmidt, A. Giese, and J. Herms. 2017. Seeding and transgenic overexpression of alpha-synuclein triggers dendritic spine pathology in the neocortex. *EMBO Mol. Med.* 9:716–731. https://doi.org/10.15252/emmm.201607305

Boissière, F., S. Hunot, B. Faucheux, C. Duyckaerts, J.J. Hauw, Y. Agid, and E.C. Hirsch. 1997. Nuclear translocation of NF-kappaB in cholinergic neurons of patients with Alzheimer's disease. *Neuroreport.* 8:2849–2852. https://doi.org/10.1097/00001756-199709080-00009

Bowman, A.W., and A. Azzalini. 1997. Applied smoothing techniques for data analysis: the kernel approach with S-Plus illustrations. Oxford University Press, Oxford, UK.

Burguete, A.S., S. Almeida, F.B. Gao, R. Kalb, M.R. Akins, and N.M. Bonini. 2015. GGGGCC microsatellite RNA is neuritically localized, induces branching defects, and perturbs transport granule function. *eLife.* 4: e08881. https://doi.org/10.7554/eLife.08881

Cao, S., X. Zhang, J.P. Edwards, and D.M. Mosser. 2006. NF-kappaB1 (p50) homodimers differentially regulate pro- and anti-inflammatory cytokines in macrophages. *J. Biol. Chem.* 281:26041–26050. https://doi.org/10.1074/jbc.M602222200

Chen, C.H., W. Zhou, S. Liu, Y. Deng, F. Cai, M. Tone, Y. Tone, Y. Tong, and W. Song. 2012. Increased NF-κB signalling up-regulates BACE1 expression and its therapeutic potential in Alzheimer's disease. *Int. J. Neuropsychopharmacol.* 15:77–90. https://doi.org/10.1017/S1461145711000149

Chinchore, Y., G.F. Gerber, and P.J. Dolph. 2012. Alternative pathway of cell death in Drosophila mediated by NF-κB transcription factor Relish. *Proc. Natl. Acad. Sci. USA.* 109:E605–E612. https://doi.org/10.1073/pnas.1110666109

Chuang, C.Y., C.C. Yang, B.W. Soong, C.Y. Yu, S.H. Chen, H.P. Huang, and H.C. Kuo. 2019. Modeling spinocerebellar ataxias 2 and 3 with iPSCs reveals a role for glutamate in disease pathology. *Sci. Rep.* 9:1166. https://doi.org/10.1038/s41598-018-37774-2

Chung, C.G., M.J. Kwon, K.H. Jeon, D.Y. Hyeon, M.H. Han, J.H. Park, I.J. Cha, J.H. Cho, K. Kim, S. Rho, et al. 2017. Golgi Outpost Synthesis Impaired by Toxic Polyglutamine Proteins Contributes to Dendritic Pathology in Neurons. *Cell Rep.* 20:356–369. https://doi.org/10.1016/j.celrep.2017.06.059

Chung, C.G., H. Lee, and S.B. Lee. 2018. Mechanisms of protein toxicity in neurodegenerative diseases. *Cell. Mol. Life Sci.* 75:3159–3180. https://doi.org/10.1007/s00018-018-2854-4

Clarke, J.R., N.M. Lyra E Silva, C.P. Figueiredo, R.L. Frozza, J.H. Ledo, D. Beckman, C.K. Katashima, D. Razolli, B.M. Carvalho, R. Frazão, et al. 2015. Alzheimer-associated Aβ oligomers impact the central nervous system to induce peripheral metabolic deregulation. *EMBO Mol. Med.* 7: 190–210. https://doi.org/10.15252/emmm.201404183

De Gregorio, E., P.T. Spellman, P. Tzou, G.M. Rubin, and B. Lemaitre. 2002. The Toll and Imd pathways are the major regulators of the immune response in Drosophila. *EMBO J.* 21:2568–2579. https://doi.org/10.1093/emboj/21.11.2568

Ghosh, A., A. Roy, X. Liu, J.H. Kordower, E.J. Mufson, D.M. Hartley, S. Ghosh, R.L. Mosley, H.E. Gendelman, and K. Pahan. 2007. Selective inhibition of NF-kappaB activation prevents dopaminergic neuronal loss in a mouse model of Parkinson's disease. *Proc. Natl. Acad. Sci. USA.* 104: 18754–18759. https://doi.org/10.1073/pnas.0704908104

Goodman, L.D., M. Prudencio, N.J. Kramer, L.F. Martinez-Ramirez, A.R. Srinivasan, M. Lan, M.J. Parisi, Y. Zhu, J. Chew, C.N. Cook, et al. 2019. Toxic expanded GGGGCC repeat transcription is mediated by the PAF1 complex in C9orf72-associated FTD. *Nat. Neurosci.* 22:863–874. https://doi.org/10.1038/s41593-019-0396-1

Gorrie, G.H., F. Fecto, D. Radzicki, C. Weiss, Y. Shi, H. Dong, H. Zhai, R. Fu, E. Liu, S. Li, et al. 2014. Dendritic spinopathy in transgenic mice expressing ALS/dementia-linked mutant UBQLN2. *Proc. Natl. Acad. Sci. USA.* 111:14524–14529. https://doi.org/10.1073/pnas.1405741111

Graveland, G.A., R.S. Williams, and M. DiFiglia. 1985. Evidence for degenerative and regenerative changes in neostriatal spiny neurons in Huntington's disease. *Science.* 227:770–773. https://doi.org/10.1126/science.3155875

Gutierrez, H., V.A. Hale, X. Dolcet, and A. Davies. 2005. NF-kappaB signalling regulates the growth of neural processes in the developing PNS and CNS. *Development.* 132:1713–1726. https://doi.org/10.1242/dev.01702

Helenius, M., M. Hänninen, S.K. Lehtinen, and A. Salminen. 1996. Changes associated with aging and replicative senescence in the regulation of transcription factor nuclear factor-kappa B. *Biochem. J.* 318:603–608. https://doi.org/10.1042/bj3180603

Heneka, M.T., M.J. Carson, J. El Khoury, G.E. Landreth, F. Brosseron, D.L. Feinstein, A.H. Jacobs, T. Wyss-Coray, J. Vitorica, R.M. Ransohoff, et al. 2015. Neuroinflammation in Alzheimer's disease. *Lancet Neurol.* 14: 388–405. https://doi.org/10.1016/S1474-4422(15)70016-5

Hinz, M., P. Löser, S. Mathas, D. Krappmann, B. Dörken, and C. Scheidereit. 2001. Constitutive NF-kappaB maintains high expression of a characteristic gene network, including CD40, CD86, and a set of antiapoptotic genes in Hodgkin/Reed-Sternberg cells. *Blood.* 97:2798–2807. https://doi.org/10.1182/blood.V97.9.2798

Hirsch, E.C., and S. Hunot. 2009. Neuroinflammation in Parkinson's disease: a target for neuroprotection? *Lancet Neurol.* 8:382–397. https://doi.org/10.1016/S1474-4422(09)70062-6

Hiscott, J., J. Marois, J. Garoufalis, M. D'Addario, A. Roulston, I. Kwan, N. Pepin, J. Lacoste, H. Nguyen, G. Bensi, et al. 1993. Characterization of a functional NF-kappa B site in the human interleukin 1 beta promoter: evidence for a positive autoregulatory loop. *Mol. Cell. Biol.* 13:6231–6240. https://doi.org/10.1128/MCB.13.10.6231

Hsiao, H.Y., Y.C. Chen, H.M. Chen, P.H. Tu, and Y. Chern. 2013. A critical role of astrocyte-mediated nuclear factor-κB-dependent inflammation in Huntington's disease. *Hum. Mol. Genet.* 22:1826–1842. https://doi.org/10.1093/hmg/ddt036

Hunot, S., B. Brugg, D. Ricard, P.P. Michel, M.P. Muriel, M. Ruberg, B.A. Faucheux, Y. Agid, and E.C. Hirsch. 1997. Nuclear translocation of NF-kappaB is increased in dopaminergic neurons of patients with parkinson disease. *Proc. Natl. Acad. Sci. USA.* 94:7531–7536. https://doi.org/10.1073/pnas.94.14.7531

Jan, Y.N., and L.Y. Jan. 2010. Branching out: mechanisms of dendritic arborization. *Nat. Rev. Neurosci.* 11:316–328. https://doi.org/10.1038/nrn2836

Ji, Y., C. Thomas, N. Tulin, N. Lodhi, E. Boamah, V. Kolenko, and A.V. Tulin. 2016. Charon Mediates Immune Deficiency-Driven PARP-1-Dependent Immune Responses in Drosophila. *J. Immunol.* 197:2382–2389. https://doi.org/10.4049/jimmunol.1600994

Kawaguchi, Y., T. Okamoto, M. Taniwaki, M. Aizawa, M. Inoue, S. Katayama, H. Kawakami, S. Nakamura, M. Nishimura, I. Akiguchi, et al. 1994. CAG expansions in a novel gene for Machado-Joseph disease at chromosome 14q32.1. *Nat. Genet.* 8:221–228. https://doi.org/10.1038/ng1194-221

Khoshnan, A., J. Ko, E.E. Watkin, L.A. Paige, P.H. Reinhart, and P.H. Patterson. 2004. Activation of the IkappaB kinase complex and nuclear factor-kappaB contributes to mutant huntingtin neurotoxicity. *J. Neurosci.* 24: 7999–8008. https://doi.org/10.1523/JNEUROSCI.2675-04.2004

Knobloch, M., and I.M. Mansuy. 2008. Dendritic spine loss and synaptic alterations in Alzheimer's disease. *Mol. Neurobiol.* 37:73–82. https://doi.org/10.1007/s12035-008-8018-z

Kounatidis, I., S. Chtarbanova, Y. Cao, M. Hayne, D. Jayanth, B. Ganetzky, and P. Ligoxygakis. 2017. NF-κB Immunity in the Brain Determines Fly Lifespan in Healthy Aging and Age-Related Neurodegeneration. *Cell Rep.* 19:836–848. https://doi.org/10.1016/j.celrep.2017.04.007

Kweon, J.H., S. Kim, and S.B. Lee. 2017. The cellular basis of dendrite pathology in neurodegenerative diseases. *BMB Rep.* 50:5–11. https://doi.org/10.5483/BMBRep.2017.50.1.131

Kwon, M.J., M.H. Han, J.A. Bagley, D.Y. Hyeon, B.S. Ko, Y.M. Lee, I.J. Cha, S.Y. Kim, D.Y. Kim, H.M. Kim, et al. 2018. Coiled-coil structure-dependent interactions between polyQ proteins and Foxo lead to dendrite pathology and behavioral defects. *Proc. Natl. Acad. Sci. USA.* 115: E10748–E10757. https://doi.org/10.1073/pnas.1807206115

Lee, S.B., J.A. Bagley, H.Y. Lee, L.Y. Jan, and Y.N. Jan. 2011. Pathogenic polyglutamine proteins cause dendrite defects associated with specific actin cytoskeletal alterations in Drosophila. *Proc. Natl. Acad. Sci. USA.* 108:16795–16800. https://doi.org/10.1073/pnas.1113573108

Marcora, E., and M.B. Kennedy. 2010. The Huntington's disease mutation impairs Huntingtin's role in the transport of NF-κB from the synapse to the nucleus. *Hum. Mol. Genet.* 19:4373–4384. https://doi.org/10.1093/hmg/ddq358

Maruyama, H., H. Morino, H. Ito, Y. Izumi, H. Kato, Y. Watanabe, Y. Kinoshita, M. Kamada, H. Nodera, H. Suzuki, et al. 2010. Mutations of optineurin in amyotrophic lateral sclerosis. *Nature.* 465:223–226. https://doi.org/10.1038/nature08971

May, S., D. Hornburg, M.H. Schludi, T. Arzberger, K. Rentzsch, B.M. Schwenk, F.A. Grässer, K. Mori, E. Kremmer, J. Banzhaf-Strathmann, et al. 2014. C9orf72 FTLD/ALS-associated Gly-Ala dipeptide repeat proteins cause neuronal toxicity and Unc119 sequestration. *Acta Neuropathol.* 128:485–503. https://doi.org/10.1007/s00401-014-1329-4

McNeill, T.H., S.A. Brown, J.A. Rafols, and I. Shoulson. 1988. Atrophy of medium spiny I striatal dendrites in advanced Parkinson's disease. *Brain Res.* 455:148–152. https://doi.org/10.1016/0006-8993(88)90124-2

Mizielinska, S., S. Grönke, T. Niccoli, C.E. Ridler, E.L. Clayton, A. Devoy, T. Moens, F.E. Norona, I.O.C. Woollacott, J. Pietrzyk, et al. 2014. C9orf72 repeat expansions cause neurodegeneration in Drosophila through arginine-rich proteins. *Science.* 345:1192–1194. https://doi.org/10.1126/science.1256800

Moens, T.G., T. Niccoli, K.M. Wilson, M.L. Atilano, N. Birsa, L.M. Gittings, B.V. Holbling, M.C. Dyson, A. Thoeng, J. Neeves, et al. 2019. C9orf72 arginine-rich dipeptide proteins interact with ribosomal proteins in vivo to induce a toxic translational arrest that is rescued by eIF1A. *Acta Neuropathol.* 137:487–500. https://doi.org/10.1007/s00401-018-1946-4

Mogi, M., M. Harada, T. Kondo, P. Riederer, H. Inagaki, M. Minami, and T. Nagatsu. 1994. Interleukin-1 beta, interleukin-6, epidermal growth factor and transforming growth factor-alpha are elevated in the brain from parkinsonian patients. *Neurosci. Lett.* 180:147–150. https://doi.org/10.1016/0304-3940(94)90508-8

Mogi, M., T. Kondo, Y. Mizuno, and T. Nagatsu. 2007. p53 protein, interferon-gamma, and NF-kappaB levels are elevated in the parkinsonian brain. *Neurosci. Lett.* 414:94–97. https://doi.org/10.1016/j.neulet.2006.12.003

Nakazawa, S., D. Oikawa, R. Ishii, T. Ayaki, H. Takahashi, H. Takeda, R. Ishitani, K. Kamei, I. Takeyoshi, H. Kawakami, et al. 2016. Linear ubiquitination is involved in the pathogenesis of optineurin-associated amyotrophic lateral sclerosis. *Nat. Commun.* 7:12547. https://doi.org/10.1038/ncomms12547

Ochaba, J., G. Fote, M. Kachemov, S. Thein, S.Y. Yeung, A.L. Lau, S. Hernandez, R.G. Lim, M. Casale, M.J. Neel, et al. 2019. IKKβ slows Huntington's disease progression in R6/1 mice. *Proc. Natl. Acad. Sci. USA.* 116: 10952–10961. https://doi.org/10.1073/pnas.1814246116

Osorio, F.G., C. Bárcena, C. Soria-Valles, A.J. Ramsay, F. de Carlos, J. Cobo, A. Fueyo, J.M. Freije, and C. López-Otín. 2012. Nuclear lamina defects cause ATM-dependent NF-κB activation and link accelerated aging to a systemic inflammatory response. *Genes Dev.* 26:2311–2324. https://doi.org/10.1101/gad.197954.112

Philips, T., and W. Robberecht. 2011. Neuroinflammation in amyotrophic lateral sclerosis: role of glial activation in motor neuron disease. *Lancet Neurol.* 10:253–263. https://doi.org/10.1016/S1474-4422(11)70015-1

Pizzi, M., F. Goffi, F. Boroni, M. Benarese, S.E. Perkins, H.C. Liou, and P. Spano. 2002. Opposing roles for NF-kappa B/Rel factors p65 and c-Rel in the modulation of neuron survival elicited by glutamate and interleukin-1beta. *J. Biol. Chem.* 277:20717–20723. https://doi.org/10.1074/jbc.M201014200

Riedl, J., and M. Louis. 2012. Behavioral neuroscience: Crawling is a no-brainer for fruit fly larvae. *Curr. Biol.* 22:R867–R869. https://doi.org/10.1016/j.cub.2012.08.018

Sarnico, I., A. Lanzillotta, F. Boroni, M. Benarese, M. Alghisi, M. Schwaninger, I. Inta, L. Battistin, P. Spano, and M. Pizzi. 2009. NF-kappaB p50/RelA and c-Rel-containing dimers: opposite regulators of neuron vulnerability to ischaemia. *J. Neurochem.* 108:475–485. https://doi.org/10.1111/j.1471-4159.2008.05783.x

Shih, R.H., C.Y. Wang, and C.M. Yang. 2015. NF-kappaB Signaling Pathways in Neurological Inflammation: A Mini Review. *Front. Mol. Neurosci.* 8:77. https://doi.org/10.3389/fnmol.2015.00077

Soós, J., J.I. Engelhardt, L. Siklós, L. Havas, and K. Majtényi. 2004. The expression of PARP, NF-kappa B and parvalbumin is increased in Parkinson disease. *Neuroreport.* 15:1715–1718. https://doi.org/10.1097/01.wnr.0000136175.51954.ce

Spires, T.L., M. Meyer-Luehmann, E.A. Stern, P.J. McLean, J. Skoch, P.T. Nguyen, B.J. Bacskai, and B.T. Hyman. 2005. Dendritic spine abnormalities in amyloid precursor protein transgenic mice demonstrated by gene transfer and intravital multiphoton microscopy. *J. Neurosci.* 25: 7278–7287. https://doi.org/10.1523/JNEUROSCI.1879-05.2005

Stöven, S., I. Ando, L. Kadalayil, Y. Engström, and D. Hultmark. 2000. Activation of the Drosophila NF-kappaB factor Relish by rapid endoproteolytic cleavage. *EMBO Rep.* 1:347–352. https://doi.org/10.1093/embo-reports/kvd072

Tan, L., P. Schedl, H.J. Song, D. Garza, and M. Konsolaki. 2008. The Toll-->NFkappaB signaling pathway mediates the neuropathological effects of the human Alzheimer's Abeta42 polypeptide in Drosophila. *PLoS One.* 3:e3966. https://doi.org/10.1371/journal.pone.0003966

Tanji, T., E.Y. Yun, and Y.T. Ip. 2010. Heterodimers of NF-kappaB transcription factors DIF and Relish regulate antimicrobial peptide genes in Drosophila. *Proc. Natl. Acad. Sci. USA.* 107:14715–14720. https://doi.org/10.1073/pnas.1009473107

Terai, K., A. Matsuo, and P.L. McGeer. 1996. Enhancement of immunoreactivity for NF-kappa B in the hippocampal formation and cerebral cortex of Alzheimer's disease. *Brain Res.* 735:159–168. https://doi.org/10.1016/0006-8993(96)00310-1

Tilstra, J.S., A.R. Robinson, J. Wang, S.Q. Gregg, C.L. Clauson, D.P. Reay, L.A. Nasto, C.M. St Croix, A. Usas, N. Vo, et al. 2012. NF-κB inhibition delays DNA damage-induced senescence and aging in mice. *J. Clin. Invest.* 122: 2601–2612. https://doi.org/10.1172/JCI45785

Toonen, L.J.A., M. Overzier, M.M. Evers, L.G. Leon, S.A.J. van der Zeeuw, H. Mei, S.M. Kielbasa, J.J. Goeman, K.M. Hettne, O.T. Magnusson, et al. 2018. Transcriptional profiling and biomarker identification reveal tissue specific effects of expanded ataxin-3 in a spinocerebellar ataxia type 3 mouse model. *Mol. Neurodegener.* 13:31. https://doi.org/10.1186/s13024-018-0261-9

Träger, U., R. Andre, N. Lahiri, A. Magnusson-Lind, A. Weiss, S. Grueninger, C. McKinnon, E. Sirinathsinghji, S. Kahlon, E.L. Pfister, et al. 2014. HTT-lowering reverses Huntington's disease immune dysfunction caused by NFκB pathway dysregulation. *Brain.* 137:819–833. https://doi.org/10.1093/brain/awt355

Wiklund, M.L., S. Steinert, A. Junell, D. Hultmark, and S. Stöven. 2009. The N-terminal half of the Drosophila Rel/NF-kappaB factor Relish, REL-68, constitutively activates transcription of specific Relish target genes. *Dev. Comp. Immunol.* 33:690–696. https://doi.org/10.1016/j.dci.2008.12.002

Xu, Z., M. Poidevin, X. Li, Y. Li, L. Shu, D.L. Nelson, H. Li, C.M. Hales, M. Gearing, T.S. Wingo, and P. Jin. 2013. Expanded GGGGCC repeat RNA associated with amyotrophic lateral sclerosis and frontotemporal dementia causes neurodegeneration. *Proc. Natl. Acad. Sci. USA.* 110: 7778–7783. https://doi.org/10.1073/pnas.1219643110

Zeng, L., D. Zhang, H.S. McLoughlin, A.J. Zalon, L. Aravind, and H.L. Paulson. 2018. Loss of the Spinocerebellar Ataxia type 3 disease protein ATXN3 alters transcription of multiple signal transduction pathways. *PLoS One.* 13:e0204438. https://doi.org/10.1371/journal.pone.0204438

Supplemental material

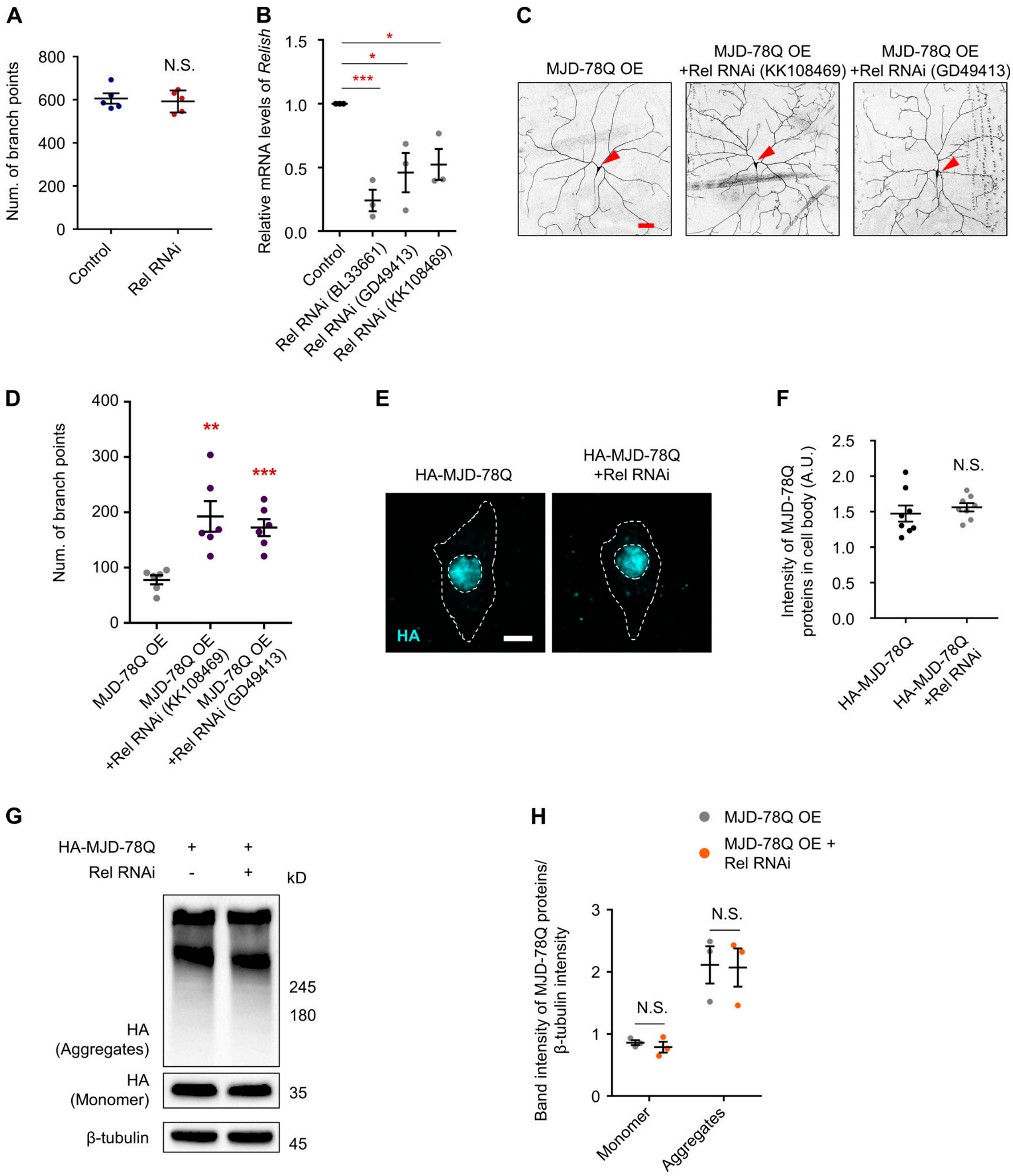

Figure S1. **Restoration of MJD-78Q–induced dendrite defects by knockdown of Relish. (A)** Quantification of the number of dendrite branch points in control C4da neurons and C4da neurons expressing Relish RNAi (BL33661) alone. N.S., not significant by Student's *t* test; error bars, SEM; *n* = 5 neurons. **(B)** Quantification of band intensities of RT-PCR products reflecting mRNA level of *Relish* in control larvae and those expressing Relish RNAi lines (BL33661, GD49413, and KK108469; *Hsp70*-Gal4/+, *Hsp70*-Gal4/*UAS-Rel RNAi* [BL33661], *UAS-Rel RNAi* [GD49413]/+;*Hsp70*-Gal4/+, and *UAS-Rel RNAi* [KK108469]/+; *Hsp70*-Gal4/+). *, $P < 0.05$; ***, $P < 1.0 \times 10^{-3}$ by Student's *t* test; error bars, SEM; *n* = 3 independent experiments. **(C)** Representative images of C4da neurons expressing MJD-78Q (left), co-overexpressing MJD-78Q + Relish RNAi (KK108469, middle), or MJD-78Q + Relish RNAi (GD49413, right). (*UAS-CD4tdGFP/+;ppk-gal4,UAS-MJD-78Q/+*, *UAS-CD4tdGFP/UAS-Rel RNAi* [KK108469];*ppk-gal4,UAS-MJD-78Q/+*, and *UAS-CD4tdGFP/UAS-Rel RNAi* [GD49413];*ppk-gal4,UAS-MJD-78Q/+*). Red-colored arrowheads indicate cell bodies of C4da neurons. Scale bar, 50 µm. **(D)** Quantification of the number of dendrite branch points in C4da neurons expressing transgenes described in C. **, $P < 1.0 \times 10^{-2}$; ***, $P < 1.0 \times 10^{-3}$ by Student's *t* test; error bars, SEM; *n* = 6 neurons. **(E)** Representative images showing MJD-78Q proteins in C4da neurons expressing denoted transgenes. (*UAS-CD4tdGFP/+;ppk-gal4,UAS-HA-MJD-78Q/+* and *UAS-CD4tdGFP/+;ppk-gal4,UAS-HA-MJD-78Q/UAS-Rel RNAi* [BL33661]). MJD-78Q proteins were detected by anti-HA antibody. Outer and inner dashed lines (white) indicate outlines of cell body and nucleus, respectively. Scale bar, 5 µm. **(F)** Quantification of intensity of MJD-78Q proteins in cell body of C4da neurons expressing denoted transgenes in E. N.S., not significant by Student's *t* test; error bars, SEM; *n* = 8 neurons. **(G)** Representative images of Western blot analysis using whole cell lysates of adult fly heads (*UAS-HA-MJD-78Q/+;elav-gal4/+* and *UAS-HA-MJD-78Q/+;elav-gal4/UAS-Rel RNAi* [BL33661]). Aggregates and monomers of MJD-78Q proteins were detected using anti-HA antibody (3F10), and β-tubulin (E7) was used as a loading control. **(H)** Quantification of band intensities in G reflecting amounts of MJD-78Q proteins. The quantified band intensity of MJD-78Q was normalized to that of β-tubulin in each sample. N.S., not significant by Student's *t* test; error bars, SEM; *n* = 3 independent experiments.

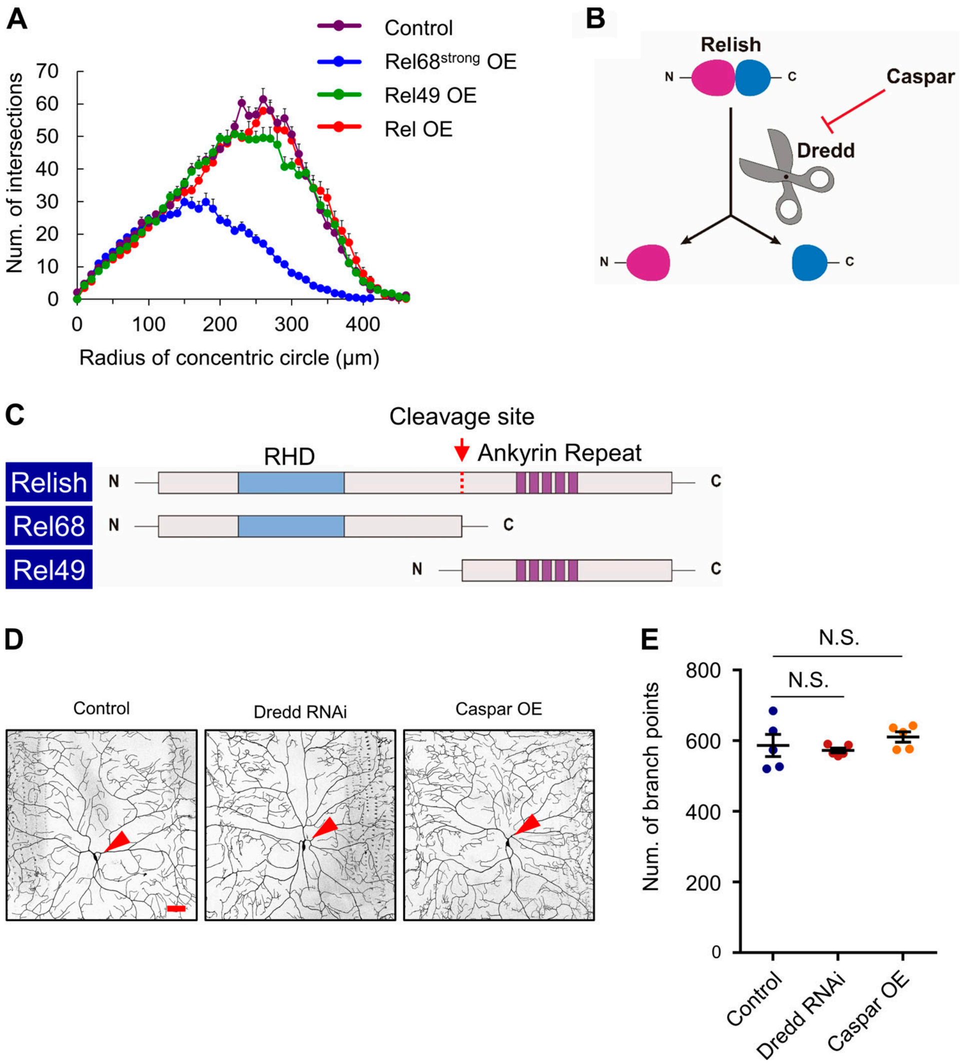

Figure S2. **Endoproteolytic cleavage of Relish controlled by Dredd and Caspar. (A)** Sholl analysis showing the number of intersections between dendrites of C4da neurons and the concentric circle from cell body to a radius of 460 µm, measured in intervals of 10 µm. Each plot indicates mean intersection value. Error bars, ±SEM; *n* ≥ 7 neurons. The number of neurons tested are as follows: Control = 9, Rel68^{strong} = 11, Rel49 = 7, and Relish = 8. **(B)** Illustration showing regulation of Relish cleavage by Dredd and Caspar. **(C)** Illustration showing domain structures of Relish, Rel68, and Rel49. **(D)** Representative images of control C4da neuron (left) and C4da neuron expressing Dredd RNAi (middle) or Caspar (right). (*UAS-CD4tdGFP/+;ppk-gal4/+*, *UAS-CD4tdGFP/+;ppk-gal4/UAS-Dredd RNAi*, and *UAS-CD4tdGFP/UAS-2xV5-Caspar;ppk-gal4/+*). Red-colored arrowheads indicate cell bodies of C4da neurons. Scale bar, 50 µm. **(E)** Quantification of the number of dendrite branch points in C4da neuron expressing transgenes described in D. N.S., not significant by one-way ANOVA with Tukey post hoc test; error bars, SEM; *n* = 5 neurons.

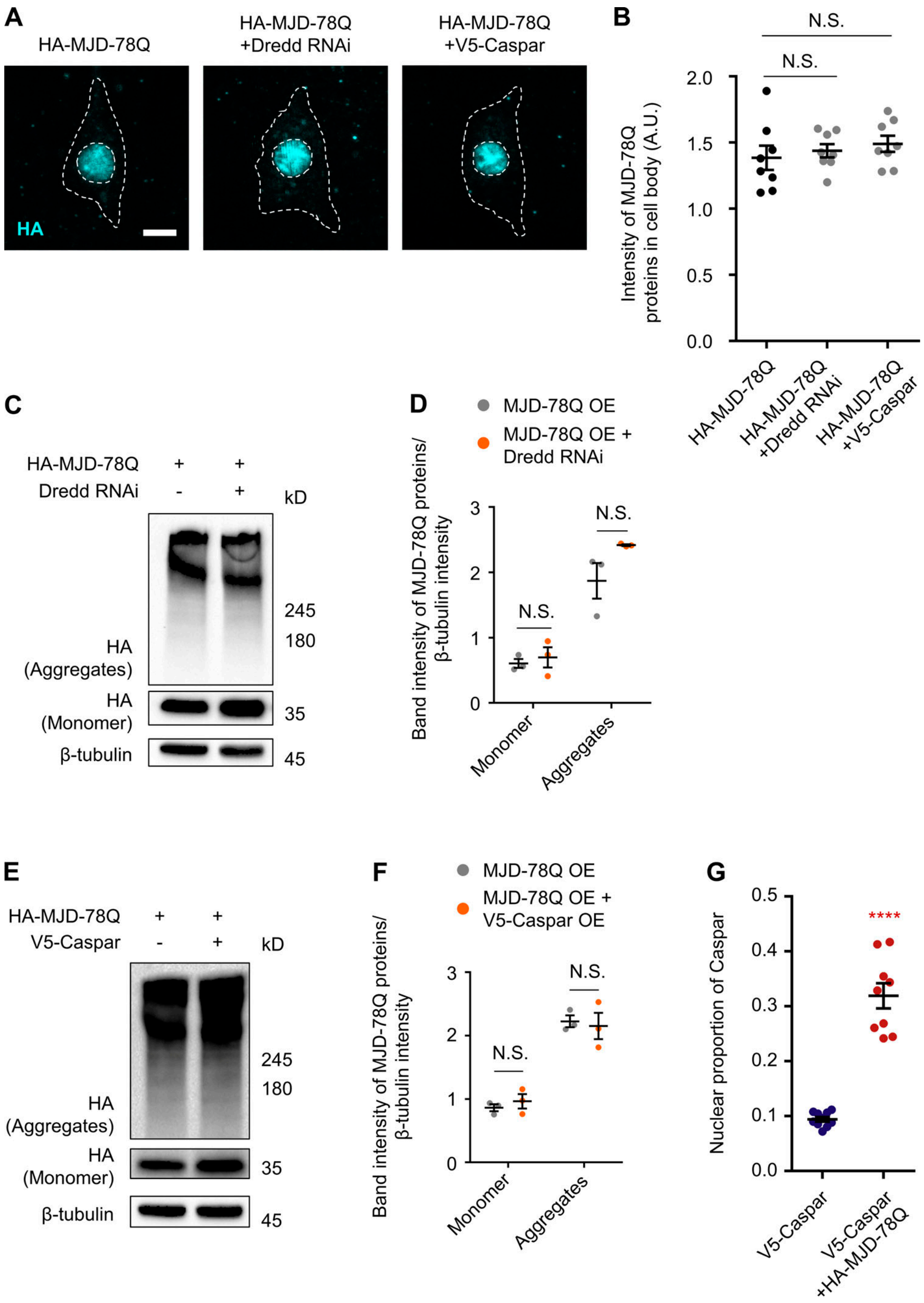

Figure S3. **No changes in the amount of toxic MJD polyQ proteins by Dredd RNAi or Caspar overexpression. (A)** Representative images showing MJD-78Q proteins in C4da neurons expressing denoted transgenes (*UAS-CD4tdGFP/+;ppk-gal4,UAS-HA-MJD-78Q/+*, *UAS-CD4tdGFP/+;ppk-gal4,UAS-HA-MJD-78Q/UAS-Dredd RNAi*, and *UAS-CD4tdGFP/UAS-2xV5-Caspar;ppk-gal4,UAS-HA-MJD-78Q/+*). MJD-78Q proteins were detected by anti-HA antibody. Outer and inner dashed lines (white) indicate outlines of cell body and nucleus, respectively. Scale bar, 5 µm. **(B)** Quantification of intensity of MJD-78Q proteins in cell body of C4da neurons expressing denoted transgenes in A. N.S., not significant by one-way ANOVA with Tukey post hoc test; error bars, SEM; $n = 8$ neurons. A.U., arbitrary units. **(C)** Representative images of Western blot analysis using whole-cell lysates of adult fly heads (*UAS-HA-MJD-78Q/+;elav-gal4/+* and *UAS-HA-MJD-78Q/+;elav-gal4/UAS-Dredd RNAi*). Aggregates and monomers of MJD-78Q proteins were detected using anti-HA antibody (3F10), and β-tubulin (E7) was used as a loading control. **(D)** Quantification of band intensities in C reflecting amounts of MJD-78Q proteins. The quantified band intensity of MJD-78Q was normalized by that of β-tubulin in each sample. N.S., not significant by Student's *t* test; error bars, SEM; $n = 3$ independent experiments. **(E)** Representative images of Western blot analysis using whole-cell lysates of adult fly heads (*UAS-HA-MJD-78Q/+;elav-gal4/+* and *UAS-HA-MJD-78Q/UAS-2xV5-Caspar;elav-gal4/+*). Aggregates and monomers of MJD-78Q proteins were detected using anti-HA antibody (3F10), and β-tubulin (E7) was used as a loading control. **(F)** Quantification of band intensities in E reflecting amounts of MJD-78Q proteins. The quantified band intensity of MJD-78Q was normalized to that of β-tubulin in each sample. N.S., not significant by Student's *t* test; error bars, SEM; $n = 3$ independent experiments. **(G)** Quantification of nuclear proportion of Caspar in C4da neurons expressing Caspar or co-overexpressing Caspar + MJD-78Q (*UAS-CD4tdGFP/UAS-2xV5-Caspar;ppk-gal4/+* and *UAS-CD4tdGFP/UAS-2xV5-Caspar;ppk-gal4,UAS-HA-MJD-78Q/+*). ****, $P < 1.0 \times 10^{-4}$ by Student's *t* test; error bars, SEM; $n = 9$ neurons.

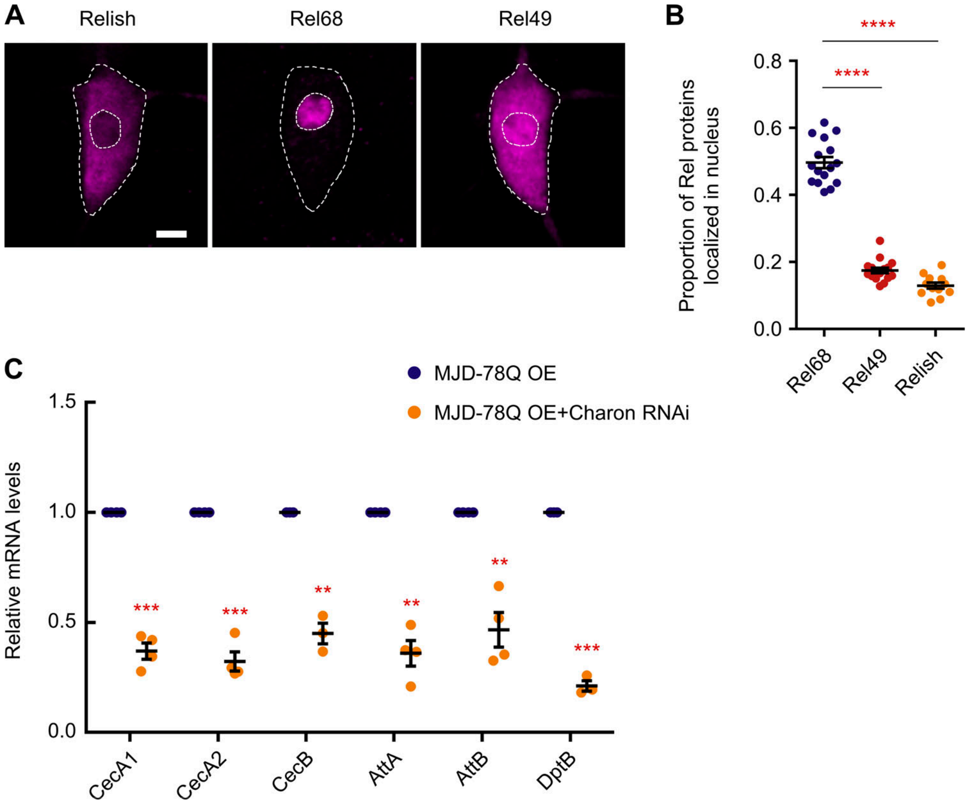

Figure S4. **Suppression of polyQ-induced up-regulation of Relish activity by knockdown of Charon. (A)** Subcellular localizations of Relish (left), Rel68 (middle), or Rel49 (right) in C4da neurons overexpressing denoted transgenes (*UAS-CD4tdGFP/+;ppk-gal4/UAS-Rel-3xHA*, *UAS-CD4tdGFP/UAS-Flag-Rel68;ppk-gal4/+*, and *UAS-CD4tdGFP/UAS-Rel49-V5;ppk-gal4/+*). Overexpressed transgenic proteins were detected using anti-HA (Relish), anti-Flag (Rel68), or anti-V5 (Rel49) antibody. Outer and inner dashed lines (white) indicate outlines of cell body and nucleus, respectively. Scale bar, 5 µm. **(B)** Proportion of nuclear localized Rel68, Rel49, or Relish in C4da neurons expressing denoted transgenes. ****, $P < 1.0 \times 10^{-4}$ by one-way ANOVA with Tukey post hoc test; error bars, SEM; $n = 12$ neurons. **(C)** Quantification of band intensities of RT-PCR products reflecting mRNA levels of transcriptional target genes of Relish (*CecA1*, *CecA2*, *CecB*, *AttA*, *AttB*, and *DptB*) in fly brains expressing MJD-78Q alone and those co-overexpressing MJD-78Q + Charon RNAi (*UAS-MJD-78Q/+;elav-gal4/+* and *UAS-MJD-78Q/UAS-Charon RNAi;elav-gal4/+*). **, $P < 1.0 \times 10^{-2}$; ***, $P < 1.0 \times 10^{-3}$ by Student's *t* test; error bars, SEM; $n = 3$ independent experiments.

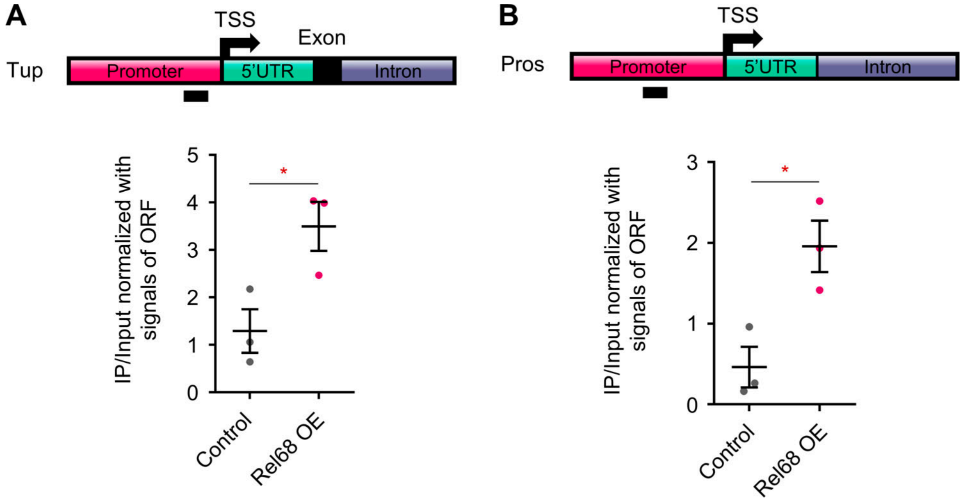

Figure S5. **Transcriptional regulation of *Tup* and *Pros* by Rel68. (A and B)** Enrichment of Rel68 in promoter region of *Tup* or *Pros* assessed by ChIP-PCR analysis. The enrichment signals (IP/Input) of promoter region were normalized with those of ORF region. *, $P < 0.05$ by Student's *t* test; error bars, SEM; $n = 3$ independent experiments (Locus amplified by primers in qPCR experiments is marked with black bars in upper panels).

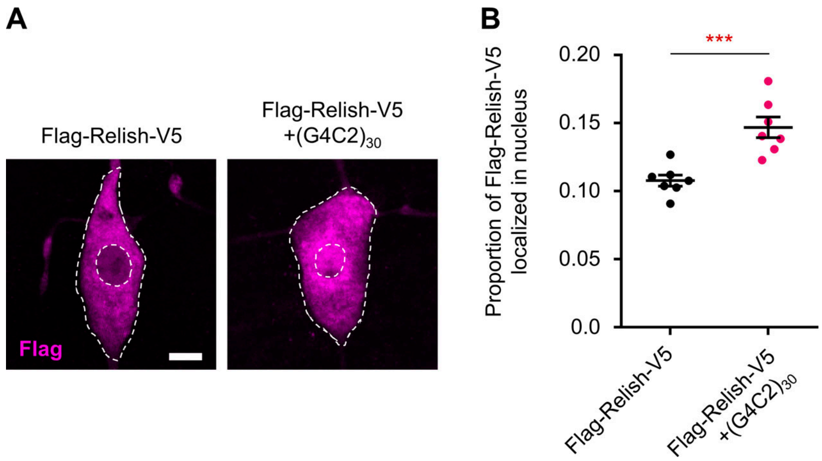

Figure S6. **Increase of N-terminal fragment of Relish in neurons expressing $(G4C2)_{30}$.** **(A)** Representative distribution patterns of Flag-Relish-V5 (detected using anti-Flag antibody) in C4da neurons expressing denoted genes (*UAS-2xFlag-Relish-2xV5/+;ppk^{1a}-gal4,UAS-CD4tdGFP/+* and *UAS-2xFlag-Relish-2xV5/UAS-$(G4C2)_{30}$;ppk^{1a}-gal4,UAS-CD4tdGFP/+*). Outer and inner dashed lines (white) indicate outlines of cell body and nucleus, respectively. Scale bar, 5 µm. **(B)** Quantification of nuclear proportion of Flag-positive Relish in C4da neurons expressing denoted gene in A. ***, $P < 1.0 \times 10^{-3}$ by Student's *t* test; error bars, SEM; *n* = 7 neurons.

Provided online are three tables. Table S1 lists studies reporting association of NF-κB with NDs and aging. Table S2 provides detailed information about RT-PCR primers for *Relish* and antimicrobial peptide genes. Table S3 includes detailed information about primers used for RT-PCR of genes involved in dendrite morphogenesis.